# Preparations and Characterization of Chitin Nanofibers and Related Materials

**July, 2014**

**Ajoy Kumar Dutta**

Department of Chemistry and Biotechnology

Graduate School of Engineering

Tottori University

# CONTENTS

# List of Figures

# List of Tables

# General Introduction

Chitin is the second most widely occurring biopolymer in the world behind cellulose, and is synthesized in quantities of approximately $10^{10}$ to $10^{11}$ tons each year.[1] Chitin is composed of $\beta$-1,4 linked *N*-acetylglucosamine units, though some deacetylation (5-10 %) is typically present in natural systems. They are structurally similar, but chitin has unique characteristics because of its C-2 acetamide group [Figure 1(a), (b)]. The major forms of chitin in animals include, the exoskeletons of crustaceans and mollusks, the backbone of squids and the cuticles of insects. [2] In recent years, chitin has attracted much attention in the scientific community because of its unusual combination of biological activities and mechanical and physical properties.[3] As such; chitin has found applications in biomedicines, foods, and cosmetics, and as nanocomposites, and electrochemical biosensors.[2, 4 - 8]

Depending on its biological origin, chitin has been found in three polymorphic forms, as $\alpha$-, $\beta$-, and $\gamma$-chitin.[9] These polymorphic forms differ in their arrangement of chains within crystalline regions, indicating different networks of hydrogen bonds. The $\alpha$-type is characterized by an anti-parallel arrangements of adjacent chains, the $\beta$-type by a parallel arrangement, and the $\gamma$-type having a mixed arrangement of chitin chains.[10] Most chitins have $\alpha$-type crystalline structure, while the $\beta$-type present in squid pen and tubeworms,[11] and the $\gamma$-type in cocoon fibers of the *Ptinus* beetle and the stomach of *Loligo*.[12] The crystallinity of chitins influences the accessibility of internal sorption sites to solvent, reducing the solubility of chitins in most common solvents.

Chitosan [Figure 1(c)] is a naturally occurring linear cationic polysaccharide generated by the deacetylation of chitin. It's environmentally friendly, non-toxic, and antimicrobial properties have led to significant interest in the biomedical applications of chitosan, including for drug deliveries, as artificial tissue scaffolds for functional tissue engineering, and for wound-healing dressings.[13-15] Chitosan has also been widely studied for its applications in food, food-film packaging, the textile industry, water purification and metal chelation.[16 - 20]

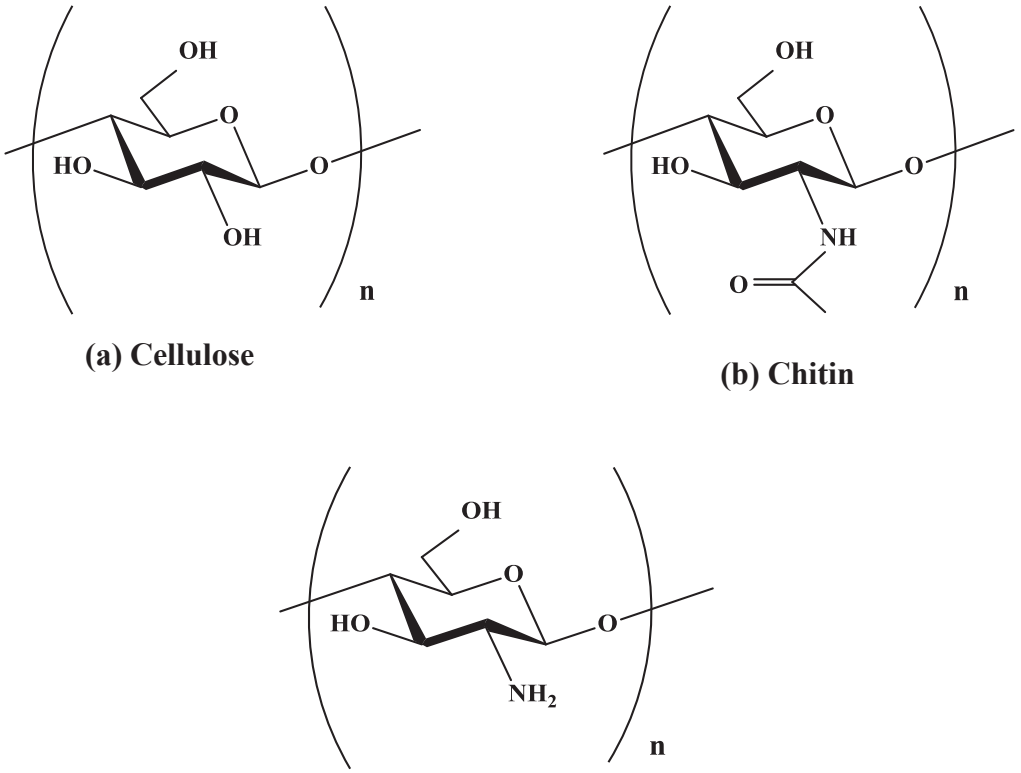


**Figure 1.** Chemical structure of (a) cellulose, (b) chitin, and (c) chitosan.

Nanofibers are typically defined as fibers smaller than 100 nm in at least one dimension. At this scale, nanofibers have a larger surface area; greater mechanical, electrical, and optical properties; and greater chemical reactivity than larger fibers. These features suggested that nanofibers may have promising applications, especially in nanofibers-reinforced composites, tissue engineering scaffolds, drug delivery, and filter media.[21 - 24] Interest has increased, however, in the production of nanofibers from biopolymers, owing to their "green" characteristics. This includes biocompatibility, and biodegradability, as well as ecological safety, low toxicity, renewability, and sustainability.[25]

Considering all of the factors, we hypothesized that the natural polymer chitin and its derivative chitosan could act as raw material in the synthesis of nanofibers. Moreover, an eco-friendly, facile process, using high pressure water jet technology, was deliberately used throughout the study to synthesize nanofibers. These nanofibers were subsequently characterized in detail, including their morphology, chemical and crystalline structure, transparency, viscosity, and mechanical properties. Finally, antimicrobial activities were generated by modifying surface of the chitin nanofibers.

Chapter 1 describes the preparation of $\alpha$-chitin nanofibers using a high pressure water jet (HPWJ) system, along with the effect of different passes on nanofibrillation. The number of passes was found to strongly affect the nanofiber morphology, molecular weight, thickness and length. Scanning probe microscopy (SPM) showed that the thickness of individualized nanofibers ranged from 4 to 6 nm. Although the mechanical properties of chitin nanofiber sheets were improved by increasing the number of passes

to 30, their chemical and crystalline structures remained unaltered even at higher passes, despite applying a high pressure of 245 MPa during each cycle.

Chapter 2 describes the preparation of $\beta$-chitin nanofibers from squid pen chitin. The morphology of these nanofibers was characterized by SPM, with the results supported by the viscosity and transmittance of nanofibers slurry. Nanofibers 3-4 nm thick were isolated, with their chemical structure remained unaffected. The crystalline structure and crystallinity of these nanofibers were maintained fully after applying HPWJ technology.

Chapter 3 describes the preparation of chitin nanocrystals (CNCs) after hydrolyzing chitin powder using hydrochloric, sulfuric and phosphoric acids generating H-CNCs, S-CNCs and P-CNCs. The dimensions of the CNCs depended on the acid to chitin ratio, as well as the hydrolysis time. The mean cross-sectional widths of H-, S- and P-CNCs were found to be 9.3 nm, 8 nm, and 7.3 nm, respectively. All forms of nanocrystals homogeneously dispersed in water, although, P-CNCs had the highest thermal stability.

Although, electrospinning is the conventional method used to extract chitosan nanofibers, Chapter 4 describes HPWJ system for nanofibers isolation. Powdered chitosan was converted into thinner nanofibers, with nanofibrillation stopped after about 10 passes. Although, thickness of these nanofibers did not change notably after 10 passes, their crystallinity decreased gradually because of the increase in high collisions forces generated during the extensive cycles of treatments. Therefore, the mechanical

properties and thermal expansion of the chitosan nanofiber sheets improved only up to 10 passes, with further treatment resulting in a deterioration of these properties.

In chapter 5, the surface of chitin nanofiber (CNF) film was modified to *N*-halamine by the reaction of the film with sodium hypochlorite solution at room temperature, endowing the film with antibacterial and antifungal properties. The amount of active chlorine content loaded on the CNF film depended on the sodium hypochlorite concentration and reaction time. FT-IR, UV-Vis, XRD, and TG analyses showed that the N-H bond was replaced by an N-Cl bond and that the reaction took place at the CNF surface. After chlorination, the characteristic nanochitin morphology was maintained. Although the active chlorine content of the film gradually decreased because of disassociation of the N-Cl bond, chlorine could be transferred to the CNF by another treatment with sodium hypochlorite solution. The chlorinated CNF film showed strong efficacies against Gram-negative and -positive bacteria, such as of *Escherichia coli* and *Staphylococcus aureus*, respectively, will kill all pathogens within 30 min. Moreover, incubation of the films with the fungi *Alternaria alternata* and *Penicillium digitatum* showed 100% and 80% inhibition of spore germination, respectively.

# Chapter 1

## Preparation of *α*-Chitin Nanofibers by High Pressure Water Jet System: Impact of Number of Passes on Nanofibrillation

### 1. 1 Introduction

Chitin, a *β*-(1→4)-linked 2-amino-2-deoxy-D-glucosamine, is a natural polysaccharide of major importance, and found mainly in two marine crustaceans, shrimp and crabs.[2] It is the second most abundant biopolymer, after cellulose, representing its huge availability throughout the world. In spite of chitin's nanofibrillar morphology and attractive properties, in particular biodegradability, biocompatibility, and non-toxicity, most chitin is thrown away as underutilized waste. Therefore, it is important to make effective use of chitin as an environmental friendly "green" material.

Chitin nanofiber has attracted attention with great interest due to their extremely large and active surface areas, while several methods have been employed to prepare them.[26 - 28] In recent years, Ifuku *et al.* effectively prepared chitin nanofibers from crab and prawn shells, in addition to mushroom cell walls.[29 - 31] The nanofibers found to have uniform morphology with 10-20 nm width and high aspect ratios. The most fascinating feature was the homogeneous dispersibility of nanofibers in water that helped to shape the fibers into desired forms. A grinder instrument was utilized to obtain chitin nanofibers. The complex hierarchical organization of chitin consisting of aggregate of

nanofibers, shown in Figure 2, was disintegrated by the shearing forces generated by a specially designed pair of grinding stones.

Recently, a novel high pressure water jet (HPWJ) system was developed by Sugino Machine Co., Ltd. to downsize materials in nano-size form.[32] Kose *et al.* prepared chitin nanofibers using this system.[33] The sample in the form of slurry was fed from the tank, as soon compressed by a hydraulic piston, and ejected at high pressure from a pair of nozzles. Atomization of chitin occurred due to the collisions of ejected pairs of jets into the chamber. However, Ifuku *et al.* stated that the nanofibrillaiton can be improved by using a milder acidic condition, in this system.[34] Moreover, chitin nanofibers from the HPWJ system are more advantageous in high-volume production, maintaining the product quality, and allowing less contamination compared with the disintegration by a grinder.

In this study, the author describes the preparation of $\alpha$-chitin nanofibers using HPWJ system, wherein 1 to 100 passes of mechanical treatments directly applied over the chitin's samples to study the effects of various passes on nanofibrillation. The morphological changes of nanofibers were investigated by scanning electron microscopy (SEM), along with their chemical structure, crystallinity, molecular weight, transparency, viscosity, and mechanical properties. Although, chitin nanofibers with desired properties are of huge demand for specific commercial applications, there had been no reports in detail.

## 1. 2 Experimental

### 1. 2. 1 Materials

*α*-Chitin powder from crab shell and acetic acid were purchased from Nakalai Tesque and Kanto Reagent, respectively, and were used as received. The acrylic monomer, poly (propylene glycol) diacrylate, was obtained from the Shin-Nakamura Chemical Co., Ltd.

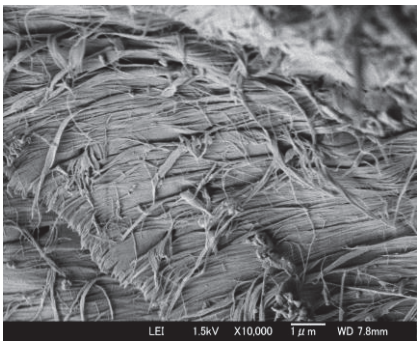


**Figure 2.** FE-SEM micrograph of *α*-chitin powder. Reproduced with permission from ref. 55. Copyright 2013, American Scientific Publishers.

### 1. 2. 2 Preparation of Chitin Nanofibers

Dry chitin powder was dispersed in water at 1 wt. %. Acetic acid was added at pH 3 to aid the nanofibrillation by cationization of the amino group. The chitin was crushed roughly with a domestic grinder. The slurry was stirred for 1 h under vacuum to remove air bubbles and then was passed through the HPWJ system (Star Burst Mini, HJP-25001S, Sugino Machine Co., Ltd.) equipped with a ball-collision chamber. The

slurry was ejected from a small nozzle having a diameter of 100 $\mu$m under high pressure (245 MPa), soon after collided with a ceramic ball with a diameter of 12.7 mm. The suspension was passed through 1, 5, 10, 30, 50, and 100 mechanical treatments, consecutively.

### 1. 2. 3 Preparation of Chitin Nanofiber Sheets and Composites

Fibrillated chitin nanofibers were dispersed in neutral water at a fiber content of 0.1 wt. %. The suspension was vacuum-filtered using a membrane filter. The obtained chitin nanofiber sheets were dried by hot-pressing at 100 $^{o}$C for 30 min. The dried sheets were cut into 5 cm × 5 cm squares of approximately 54 $\mu$m thickness and with a weight of approximately 10 mg. The squares were impregnated with bi-functional acrylic resin monomer with 2 wt. % of 2-hydroxy-2-methylpropiophenone photo initiator under reduced pressure for 24 h. The monomer-impregnated sheets were radically polymerized using UV curing equipment (Spot Cure SP-7, Ushio Inc.) for 8 min at 40 mW cm$^{-1}$. The composite films thus obtained were approximately 76 $\mu$m thick, with a fiber content of approximately 43%, calculated based on the dry weights of the squares and nanocomposites.

### 1. 2. 4 Characterization

#### 1. 2. 4. 1 Examination of Morphological Changes

For field emission scanning electron microscopic (FE-SEM) observation,

chitin powder was dried in a vacuum drying oven. The sample was coated with an approximately 2 nm layer of Pt by an ion sputter coater and observed by FE-SEM (JSM-6700F; JEOL, Ltd.) operating at 2.0 kV.

SPM observations were performed with a nanocute model SPM apparatus (Seiko Instruments Inc., Japan). Chitin nanofibers slurry was dispersed in water, with a concentration of 0.1 mg $mL^{-1}$, by an ultrasonic homogenizer just for one minute. A few drops (40 $\mu$L) of the suspension was spread on a freshly cleaved mica round disk, dried up and was examined with the help of scanning probe microscopy (SPM) observation. SPM observations were performed with a nanocute model SPM apparatus (Seiko Instruments Inc., Japan). Images were recorded as 256 × 256 pixel images for 5 $\mu$m wide square. SPM images (topographic images) were used to measure the widths of chitin nanofibers by selecting the measuring points along the fiber axes.

**1. 2. 4. 2 Determination of Chemical and Crystalline Structure**

Chemical structure of chitin nanofibers were determined by the FT-IR Spectroscopy. Infrared spectra of the samples were recorded with an FT-IR spectrophotometer (Spectrum 65, Perkin-Elmer Japan Co., Ltd.,) equipped with an ATR attachment.

X-ray diffraction studied was carried out to investigate the crystalline structure of the chitin and its nanoifbers. The profiles of the nanofibers were obtained with Ni-filtered CuK$\alpha$ from an X-ray generator (Ultima IV, Rigaku) operating at 40 kV and

30 mA. The diffraction profile was detected using X-ray goniometer scanning from 5° to 35°. The crystalline index (CI) was determined by following the equation: CI = ($I_{110}$ − $I_{am}$) × 100/$I_{110}$, where $I_{110}$ is the maximum intensity of the [110] plane and $I_{am}$ is the intensity of the amorphous diffraction at approximately16° .[35]

### 1. 2. 4. 3 Molecular weight determination

The molecular weight of chitin powder and dry chitin nanofibers were measured by the Viscosity Method with an Ubbelohde viscometer (no. 2) (Kusano Science Corporation, Tokyo, Japan) at 25 ± 0.2 °C. The specific viscosities, $\eta_{sp}$ were calculated from the following equation:

$$\eta_{SP} = \left( \frac{t}{t_o} - 1 \right) \quad (1)$$

Here the parameters t and $t_o$ were the flow times of the solvent with and without the sample, respectively. Three flow time measurements were done for each solution. The flow time data were used to calculate the specific viscosity and then the intrinsic viscosity by a linear regression of the specific viscosity versus concentration. Finally, with the intrinsic viscosity results, the Mark-Houwink-Sakurada equation was used to calculate the molecular weight of chitin and its nanofibers:

$$[\eta] = K\,(M_w)^a \quad (2)$$

Here K ($7.6\times10^{-5}$ dL $g^{-1}$) and a (0.95) are empirical constant valid for a specific polymer-solvent system at a given temperature.[36] $\eta$ is the intrinsic viscosity and $M_w$ is the molecular weight.

### 1. 2. 4. 4 Measurements of Light Transmittance and Viscosity

The light transmittances of chitin nanofiber dispersions (0.1 wt. %) and the composites were measured using a UV-Vis spectrophotometer (V550; JASCO, Tokyo, Japan).

The viscosity of the chitin nanofibers dispersions with 1.0 wt. % was measured using a Brookfield digital viscometer DV-E using spindle no. LV-4 (Brookfield Engineering Laboratories, Middleboro, MA).

### 1. 2. 4. 5 Determinations of Mechanical Properties

The Young's modulus and tensile strength analysis of sheets were evaluated using a universal testing instrument (AG-X, Shimadzu, Tokyo, Japan) for samples 50 mm long and 10 mm wide. At least five specimens were tested for their nanofiber sheets.

The coefficients of thermal expansion (CTE) of the sheets were measured with a thermomechanical analyzer (Q400, TA Instruments, Newcastle, DE). Specimens were 30 mm long and 3 mm wide, with a 20 mm span. The measurements were carried out from 30 to 165 $^{o}$C by elevating the temperature at a rate of 5$^{o}$ min$^{-1}$ in a nitrogen atmosphere in tensile mode under a load of 0.05 N. The CTE values were determined in the second run in order to dry the sample completely in the first run.

## 1. 3 Results and Discussion

### 1. 3. 1 Morphological Change of Chitin Powders

Scanning electron microscopic (SEM) observations are depicted in Figure 3. These illustrated the morphological changes of dry chitin powder into nanofibers by HPWJ, after 1to100 cycles of treatments. Even after only one pass, the chitin aggregates shown in Figure 2 were considerably disintegrated into the mixture of tens of nano-sized and submicron-sized fibers. The significant morphological change of solid chitin even after one cycle of treatment was caused by the electrostatic repulsive forces among the nanofibrills resulted from the cationization of amino groups in acidic condition. The presence of small amount of acid just crushed the strong hydrogen bonds among the fibrills in chitin. After 5 passes, chitin nanofibres morphology changed remarkably. Most of chitin aggregates were well fibrillated into nano-sized fibers. However, chitin nanofibers morphology did not change notably above 10 passes, although, a small amount of sub-micron-sized fibers continued to be fibrillated until 30 passes. Basically, at around 30 passes, nanofibrillatoin ended completely. On the other hand, the nanofibers length shortened above 30 passes, due to the strong collision forces created from the extensive cycles of treatments by the system. Therefore, morphology of chitin nanofibers persistently depended on the number of passes of HPWJ system.

### 1. 3. 3 Chemical and Crystalline Structures of Chitin Nanofibers

The FT-IR spectra of the isolated chitin nanofibers treated by the HPWJ system

after 1, 5, 10, 30, 50, and 100 passes, are depicted in Figure 4. All spectra of the obtained nanofibers were in excellent agreement with the spectrum of commercial chitin. For instance, the OH stretching band at 3424 $cm^{-1}$, the NH stretching band at 3259 $cm^{-1}$, the amide I band at 1652 and 1621 $cm^{-1}$, and the amide II band at 1554 $cm^{-1}$ of the chitin nanofibers are characteristic of $\alpha$-chitin. This suggests that the original chemical structures of chitin were maintained after the HPWJ mechanical treatments even with 100 passes.

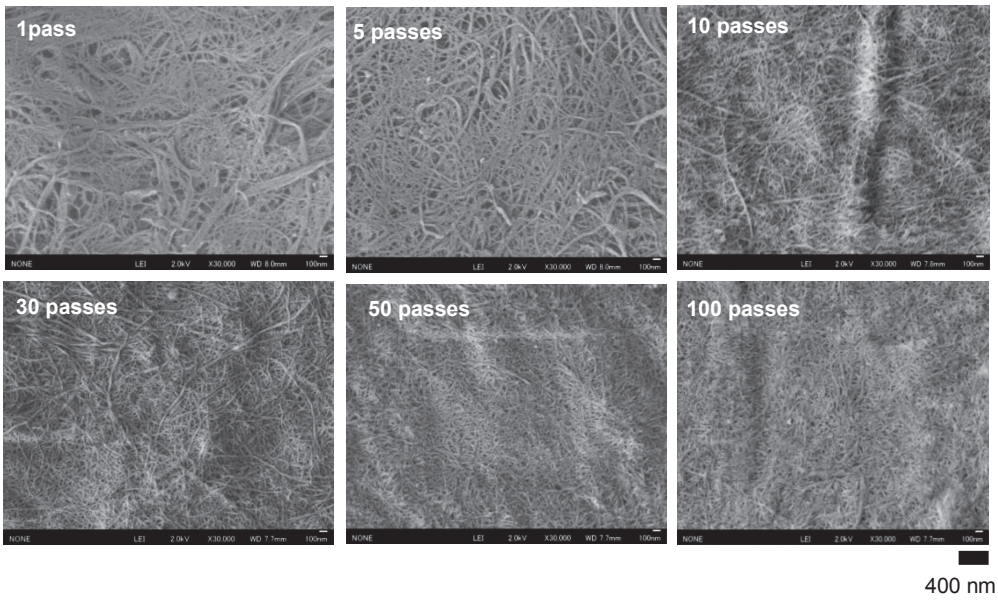


**Figure 3.** FE-SEM micrographs of $\alpha$-chitin fibers after several passes treatments by HPWJ system. The scale bar length is 400 nm. Reproduced with permission from ref. 55. Copyright 2013, American Scientific Publishers.

The crystalline structure of the nanofibers fibrillated by the HPWJ system after several passes was studied by wide-angle X-ray diffraction (WXRD). All diffraction patterns coincided closely with those of the original chitin powder. The diffraction

peaks of the chitin nanofibers observed at $2\theta$ = 9.2, 19.1, 20.9, and 23.1° corresponded to [020], [110], [120], and [130] planes, respectively. They were typical antiparallel crystal patterns of $\alpha$-chitin.[37] Thus, the original crystalline structure was maintained after the HPWJ treatments. Table I shows the degree of relative crystalline indices of chitin nanofibers determined from X-ray diffraction profiles. The degree of the relative crystalline index of the original chitin powder was 83.7%. After the HPWJ treatments from 1 to 100 passes, there were no significant differences in the relative degree of crystallinity (83.3-84.4%). This indicates that even 100 passes of HPWJ treatments did not damage the crystalline structure of the chitin fibers, although the system employed a super high-pressure water jet of 245 MPa.

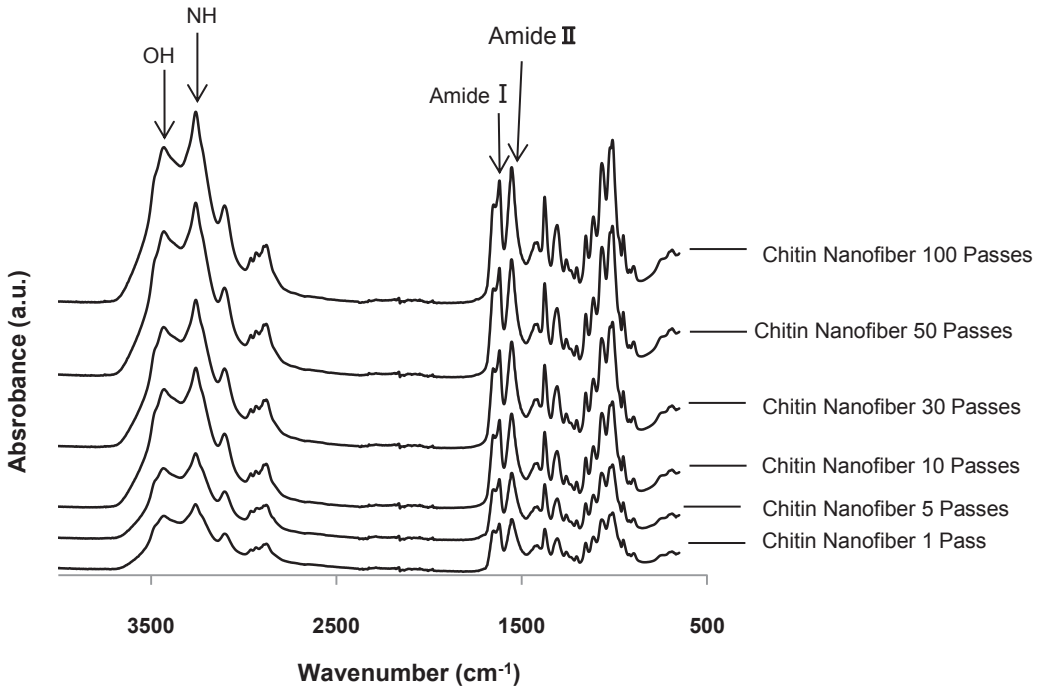


**Figure 4.** FT-IR spectra of $\alpha$-chitin nanofibers at different passes.

**Table 1.** Degree of relative crystallinity of $\alpha$-chitin nanofbers.

| **Number of Passes** | Original | 1 | 5 | 10 | 30 | 50 | 100 |
|---|---|---|---|---|---|---|---|
| **Relative Crystallinity (%)** | 83.7 | 83.3 | 84.3 | 84.3 | 84.2 | 84.4 | 84.4 |

### 1. 3. 2 Cross-sectional Widths of Chitin Nanofibers

The scanning probe microscopic (SPM) technology was used to make an authentic measurement of the chitin fibrils widths. Such measurements were made for 100 points on isolated fibrils of individual images of each passes that resulted in the histograms. The histogram reflected chitin fibrils of different thickness ranging from 3 to 8 nm. However, this was an average scenario of chitin nanofibers thickness. The effect of individual cycles of treatments by HPWJ system can be explained from Figure 5, which shows the cross-sectional widths of chitin nanifibers for individual passes. The widths of nanofibers changed drastically from 14.65 nm at 1pass to 7 nm at 5 passes and then steadily reached to 6 nm at 30 passes, after which the fiber thickness did not change remarkably. However, chitin nanofibrils with thickness of $\leqq$ 1 nm was noted surprisingly in all passes, except for 1 pass. The variations of nanofibers widths were in good agreement with the morphological changes of chitin nanofibers.

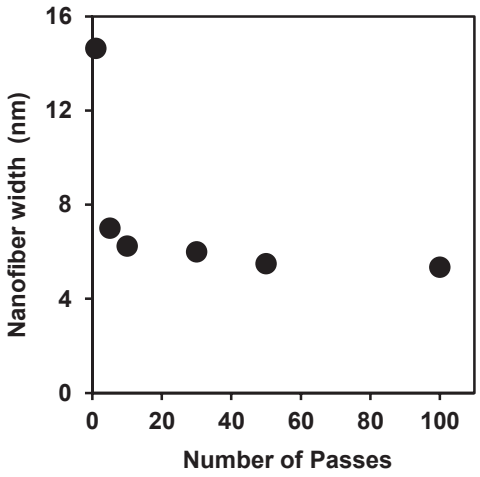


**Figure 5.** Average widths of $\alpha$-chitin nanofibers as a function of number of passes. Reproduced with permission from ref. 56. Copyright 2013, American Scientific Publishers.

### 1. 3. 4 Molecular Weights of Chitin and its Nanofibers

The Huggins viscosity relation is represented on the viscosity/concentration plots. Extrapolation yielded the intrinsic viscosity [$\eta$] for chitin and its nanofibers solutions. Molecular weight was then determined by the help of Mark-Houwink-Sakurada equation (Equation 2). Figure 6 shows the molecular weight of chitin and its nanofiber as a function of number of passes. The molecular weight of original chitin is 64.56 kDa. On the other hand, the molecular weight of chitin nanofibers decreased gradually from 1 pass (56.87 kDa) to 30 passes (50.66 kDa). These trends of molecular weight are similar with the morphological changes of chitin nanofibers. The probable reason is that the chain scissions of chitin molecules at glycosidic linkage occurred only up to a certain passes.

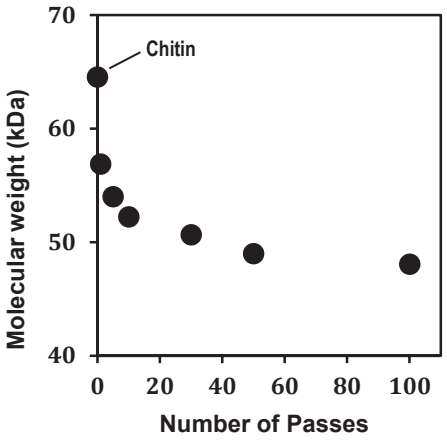


**Figure 6.** Molecular weights of $\alpha$-chitin nanofibers as a function of number of passes. Reproduced with permission from ref. 56. Copyright 2013, American Scientific Publishers.

### 1. 3. 5 Transparency and Viscosity of Chitin Nanofiber Suspensions

Figure 7 shows the regular light transmittances at 600 nm of chitin nanofiber slurry with 0.1 wt. % concentration fibrillated by the HPWJ system. Transparency is strongly associated with chitin fiber thickness because, when the solid fibers dispersed at nano level, the suspension became transparent. Generally, chitin does not disperse at all but precipitates in water, which has been a longstanding issue for the application of chitin. On the other hand, after the HPWJ treatment, chitin slurries dispersed homogeneously in water for at least a month. Thus, chitin nanofibers were easy to handle and shape into desired forms. At one pass, the light transmittance of chitin slurry was only 27.3%. At 5-30 passes, the transmittance increased steeply, to 45.9-73.9%, respectively. Above 30 passes, the transparency reached almost its peak. This trend indicates that, up to 30 mechanical treatments, chitin fibers were fibrillated into thinner

nanofibers, increasing their transparency. However, above 30 passes, the nanofibers were mostly fibrillated and further disintegration was difficult, resulting in saturated transparency. These trends agreed well with the results of SEM.

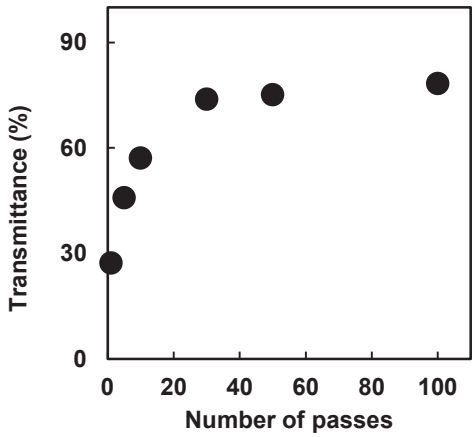


**Figure 7.** Regular light transmittance of $\alpha$-chitin nanofiber suspensions at 600 nm as a function of number of passes. Reproduced with permission from ref. 55. Copyright 2013, American Scientific Publishers.

The viscosities of the chitin nanofiber slurry with 1.0 wt. % fibrillated by the HPWJ system are shown in Figure 8, graphed against the number of passes from 1 to 100. The viscosity increased from 2010 cP at one pass to 8330 cP at 10 passes. On the other hand, above 10 passes, the viscosity decreased abruptly to 3630 cP at 100 passes. Viscosity is strongly affected by nanofibers morphology. That is, the thinner and shorter chitin nanofibers are, and the more frequently the fibers become entangled, which increases viscosity. The viscosity data indicate that, up to around 10-30 passes, the nanofibers became thinner as the number of passes increased, indicating that the nanofibrillation was mostly completed. After this, the fiber length decreased as the

fibers started to break, thereby lowering viscosity.

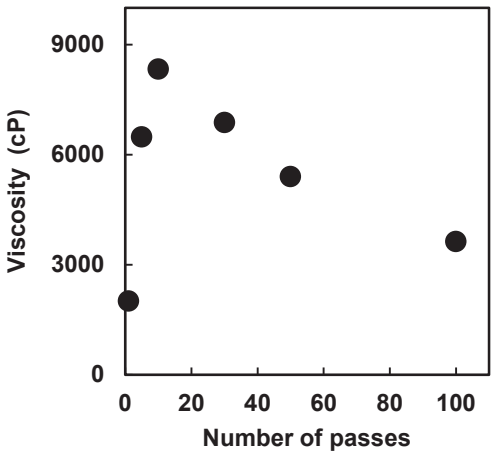


**Figure 8.** Viscosity of $\alpha$-chitin nanofiber suspensions as a function of number of passes. Reproduced with permission from ref. 55. Copyright 2013, American Scientific Publishers.

### 1. 3. 6 Characterizations of Chitin Nanofiber Sheets

Chitin nanofiber sheets were easily prepared by vacuum-filtration. Figure 9 show the density of the chitin nanofiber sheets as a function of the number of passes. At 1-10 passes, the density steeply increased to 0.69 to 0.83 g $cm^{-3}$, respectively. On the other hand, above 10 passes, the value did not change significantly. The sheet density related to the chitin nanofiber morphology shown in Figure 3. It was assessed that the thinner and shorter chitin nanofibers are, the more the nanofibers are packed densely in the sheet.

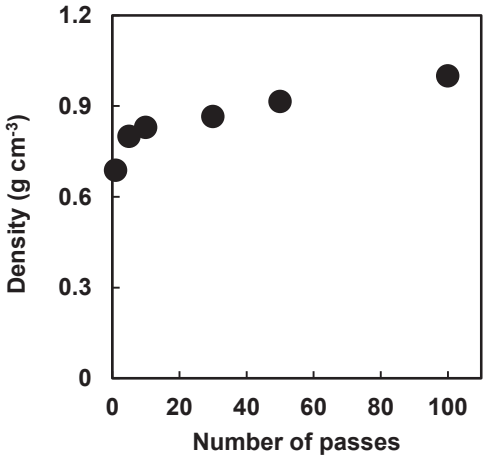


**Figure 9.** Density of $\alpha$-chitin nanofiber sheets as a function of number of passes. Reproduced with permission from ref. 55. Copyright 2013, American Scientific Publishers.

Since chitin nanofibers from crab shell have an antiparallel extended crystal structure, they have a high Young's modulus and high tensile strength.[38] Figures 10 and 11 show the tensile Young's moduli and fracture strengths, respectively, of the chitin nanofiber sheets against the number of passes from 1 to 100. As the number of passes increased, Young's moduli and fracture strengths increased. However, above 30 passes, these values did not change significantly. Basically, the fibers mechanical properties were strongly associated with nanofiber thickness. As the nanofibers became thinner, the surface area increased, which further increased the number of the hydrogen bonds between nanofibers that driven the improved mechanical properties of the chitin nanofiber sheet. Moreover, as the nanofibers became thinner, sheet density increased, which also affected mechanical properties. Since the chitin nanofiber sheets did not show a decrease in Young's moduli or in tensile strength above 30 cycles of the HPWJ treatment, the crystalline chitin fibers were not severely degraded even with 100 passes.

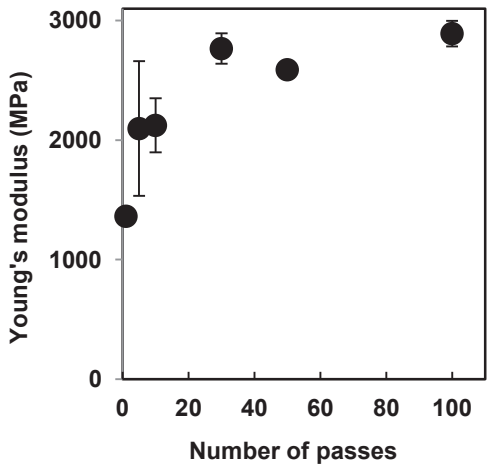


**Figure 10.** Yong's moduli of $\alpha$-chitin nanofiber sheets as a function of number of passes. Reproduced with permission from ref. 55. Copyright 2013, American Scientific Publishers.

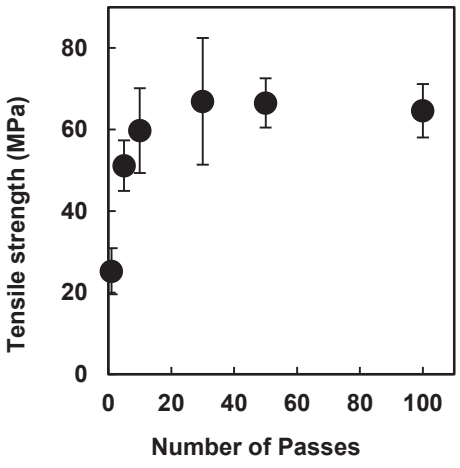


**Figure 11.** Tensile strength of $\alpha$-chitin nanofiber sheets as a function of number of passes. Reproduced with permission from ref. 55. Copyright 2013, American Scientific Publishers.

Thermal expansion is inversely related with Young's modulus. Since the Young's modulus of a chitin nanofiber (not a sheet) is estimated to be at least 150 GPa, its coefficient of thermal expansion (CTE) is very small.[38, 39] Table 2 shows the CTE values of chitin nanofiber sheets. The CTEs of all chitin nanofiber sheets were less than 10 ppm $K^{-1}$, and the HPWJ treatments did not significantly change the CTE. This result also supports that the characteristic extended crystalline structure of chitin nanofibers did not change after repeated fibrillation treatment.

**Table 2.** Coefficient of thermal expansion of $\alpha$-chitin nanofiber sheets.

| **Number of Passes** | 1 | 5 | 10 | 30 | 50 | 100 |
|---|---|---|---|---|---|---|
| **Thermal Expansion (ppm $K^{-1}$)** | 8.15 | 6.74 | 7.06 | 6.78 | 7.39 | 8.21 |

### 1. 3. 7 Transparency of Chitin Nanofibers Composite

Bacterial cellulose nanofiber-reinforced plastic films were recently reported by Yano *et al*.[40] The nanocomposite was optically transparent due to the nanofiber size effect. The results of this study could be applicable to chitin nanofibers for transparent nanocomposites.[31, 41, 42] Since the transparency depends strongly on fiber thickness, it will provide relative morphological information about the nanofibers. Thus, chitin nanofiber composite films with acrylic resin were prepared. The author chose poly (propylene glycol) diacrylate resin purposely as a matrix substance to see the

morphological changes in nanofibers. The refractive index (RI) of the resin was 1.468, which is not very close to that of chitin nanofiber (approximately 1.50). This difference causes a loss of transparency, since it causes light scattering at the interface between the nanofiber and the resin. Figure 12 shows the regular light transmittances of the composites as a function of the number of passes. The changes in transparency also indicate that the nanofibers became thinner as the number of passes increased. However, above 30 passes, the transparency of the nanocomposite was saturated, as the chitin nanofibers were mostly fibrillated. Since the light transmittance of neat poly (propylene glycol) was approximately 90% at 600 nm, optical losses of the nanocomposite film was very small, though the fiber content at 30 passes is high (43%).

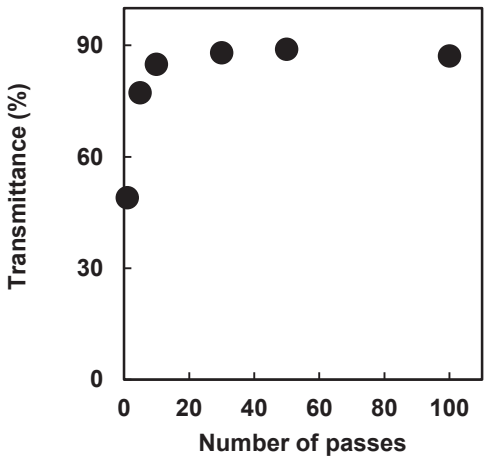


**Figure 12.** Regular light transmittance of $\alpha$-chitin nanofiber suspensions at 600 nm as a function of number of passes. Reproduced with permission from ref. 55. Copyright 2013, American Scientific Publishers.

## 1. 4 Conclusion

The effects of HPWJ system on nanofibrillation of $\alpha$-chitin at different passes was discussed in terms of several properties including the morphology, chemical structure, and crystallinity. SEM images showed that the nanofibrillation of chitin slurry significantly affected by the number of passes, although at around 10 passes disintegration ended remarkably. The thickness of nanofibers decreased as the number of passes increased gradually up to 30 passes. The light transmittance of the chitin nanofiber slurry and the nano-composite with acrylic resin showed the similar trend. On the other hand, above 30 passes, the nanofibers started to break. However, X-ray diffraction profiles of the chitin nanofibers showed that the HPWJ treatment did not reduce crystallinity, even with the high collision forces generated by HPWJ system. Therefore, mechanical properties were improved by nanofibrillation, and extensive cycles of treatment did not reduce their properties. The HPWJ system is advantageous in the commercial application of chitin nanofibers from the standpoints of quality stability, high-volume production, and low contamination. These detailed characterizations of chitin nanofibers will hope to play an important role to find out its commercial use.

# Chapter 2

## Simple Preparation of *β*-Chitin Nanofibers from Squid Pen

### 2.1 Introduction

Nature provided a variety of hierarchical structures, such as cellulose, chitin, silk, and keratin, which supported living bodies physically in plants and animals, from immemorial past. Thus, chitin occurs in nature as structural polysaccharide and is present in the exoskeleton of arthropods, in the cuticle of insects and in the cell walls of fungi. Two major naturally occurring chitin crystalline polymorphs are, namely, *α*-chitin and *β*-chitin. Most chitins have *α*-type crystal structure, while the *β*-type is present in squid pen and tubeworms.[11] In *α*-chitin, the piles of molecular chains are arranged in an antiparallel mode, while that of *β*-chitins have a parallel chain packing mode.[37, 43] Therefore, it was suggested that *α*-chitin has strong inter- and intra-sheet hydrogen bonding, compared to *β*-chitin.[44]

Nanofibers possesses several amazing characteristics, for instance, a very large surface area to volume ratio, flexibility in surface functionalities, and superior mechanical performance,[45] along with the ability to form a highly porous mesh.[46] Therefore, nanofibres has been considered as a prime candidate for many significant applications in the area of electro-optical film, nanofiber-reinforced composites, microelectronics, and tissue engineering scaffold.[47-50] Hence, the preparation of

nanofibers from various sources and their characterization, have been a matter of interest in recent time.

It was found that *β*-chitins exhibit higher reactivity in various modification reactions and higher affinity for solvents than *α*-chitin.[51 - 53] Nonetheless, there had been no reports on detail characterization of *β*-chitin nanofibers. Although, Fan *et al.* prepared *β*-chitin nanofibers by using an ultrasonic homogenizer, the isolated nanofibers could not sustain their natural crystallinity, unexpectedly. [54]

Recently, the author successfully prepared *α*-chitin nanofibers by applying novel HPWJ technology.[55] Chitin nanofibers prepared by this system had excellent morphology with fiber thickness of 4 to 6 nm, high crystallinity and mechanical properties.[56] The system was beneficial in response to excellent formability, maintaining product quality, and for low contamination. Herein, the author deliberately used the novel HPWJ technology to prepare *β*-chitin nanofibers from squid pen, under slight acidic condition. Besides, isolated nanofibers characterized in detail relating to their morphology, chemical structure, crystallinity, viscosity, and mechanical properties.

## 2. 2. Experimental

### 2. 2. 1. Materials

*β*-Chitin powder originating from squid pen was kindly provided by Koyo Chemical Co. Ltd. as a commercial product and used without further purification.

### 2. 2. 2. Preparation of Chitin Nanofibers

*β*-Chitin nanofibers were prepared according to our previously reported protocol, with slight modification.[55] In brief, squid pen chitin powder were dispersed in water at 1 wt. % and a small amount of acetic acid was added to the chitin dispersion to facilitate the nanofibrillation (pH ~ 3). The slurry was stirred for 1 h under vacuum to remove air bubbles. Finally, HPWJ system (Star Burst Mini, HJP-25001S, Sugino Machine Co., Ltd.), equipped with a ball-collision chamber, was employed to achieve successful disintegration. The slurry was ejected from a small nozzle of diameter of 100 $\mu$m under high pressure (240 MPa), soon after collided with a ceramic ball with a diameter of 12.7 mm. The slurry was passed through 1, 5, 10, 30, and 50 times mechanical treatments, on a regular basis.

### 2. 2. 3. Preparation of Chitin Nanofiber Sheets

Nano-fibrillated *β*-chitin nanofiber slurry was dispersed in distilled water at a fiber content of 0.1 wt. %. The dilute dispersion was vacuum-filtered using a membrane filter. The obtained chitin nanofiber sheets were dried by hot-pressing at 100 $^{o}$C for 30 min. The dried sheets were cut into 5 cm x 5 cm squares of approximately 45 $\mu$m thickness and with an average weight of 11 mg.

### 2. 2. 4 Characterization

Infrared spectra of the samples were recorded with an FT-IR spectrophotometer (Spectrum 65, Perkin-Elmer Japan Co., Ltd.,) equipped with an ATR attachment.

For field emission scanning electron microscopic (FE-SEM) observation, chitin powder was dried in a vacuum drying oven. The sample was coated with an approximately 2 nm layer of Pt by an ion sputter coater and observed by FE-SEM (JSM-6700F; JEOL, Ltd.) operating at 2.0 kV.

Scanning probe microscopic (SPM) observations were performed with a nanocute model SPM apparatus (Seiko Instruments Inc., Japan). Samples for SPM measurements were prepared by applying one drop of an aqueous chitin dispersion (0.1mg $mL^{-1}$) on a freshly cleaved mica round disk followed by oven drying.

X-ray diffraction profiles of the nanofibers were obtained with Ni-filtered CuK$\alpha$ from an X-ray generator (Ultima IV, Rigaku) operating at 40 kV and 30 mA. The diffraction profile was detected using X-ray goniometer scanning from $5^{o}$ to $35^{o}$. The crystalline index (CI) was determined by following the equation: $CI = (I_{110} - I_{am}) \times 100/I_{110}$, where $I_{110}$ is the maximum intensity of the [110] plane and $I_{am}$ is the intensity of the amorphous diffraction at approximately$16^{o}$.[35]

The light transmittances of chitin nanofiber dispersions with 0.1 wt. % were measured using a UV-Vis spectrophotometer (V550; JASCO, Tokyo, Japan).

The viscosity of the chitin nanofibers dispersions with 1.0 wt. % was measured using a Brookfield digital viscometer DV-E using spindle no. LV-4 (Brookfield Engineering Laboratories, Middleboro, MA).

The Young's modulus and tensile strength analysis of sheets were evaluated using a universal testing instrument (AG-X, Shimadzu, Tokyo, Japan) for samples 50 mm long and 10 mm wide. At least five specimens were tested for their nanofiber sheets.

The coefficients of thermal expansion (CTE) of the sheets were measured with a thermomechanical analyzer (Q400, TA Instruments, Newcastle, DE). Specimens were 30 mm long and 3 mm wide, with a 20 mm span. The measurements were carried out from 30 to 165 $^{o}$C by elevating the temperature at a rate of 5$^{o}$ min$^{-1}$ in a nitrogen atmosphere in tensile mode under a load of 0.05 N. The CTE values were determined in the second run in order to dry the sample completely in the first run.

## 3. 3. Results and Discussion

### 3. 3. 1. Morphological Changes of Chitin Powders

SPM micrographs are depicted in Figure 13 that postulated the deformation of dry chitin powder into nanofibers after successive HPWJ treatments. At 1 pass, aggregate of chitin fibers were observed (Fig. 13(a)). On the other hand, chitin morphology changed drastically, only after 5 passes mechanical treatments of the chitin dispersion (Fig. 13(b)). The thick aggregate of fibrous chitin surprisingly was broken down into

individualized nanofibers with a uniform network. After 5 passes, the fibers width decreased due to further fibrillation of micron-sized fibers (Fig. 13(c)). However, further mechanical treatments, especially after 10 passes, resulted in no significant changes in nannofibers formation. Although the average fibers diameters decreased to some extent, from 5.1 nm at 10 passes to 4.6 nm at 30 passes and 3.8 nm at 50 passes (Table 3). Fan *et al.* earlier reported the isolation of *β*-chitin nanofibers with 3-4 nm cross-sectional width.[54] The persisting results pointed toward the success of nano-fibrillation by the HPWJ system. Conversely, above 30 passes, the fibers started to break, due to the strong mechanical forces driven by extensive treatments, shortening their lengths. Thus, the nanofibers morphology and the number of passes are closely correlated.

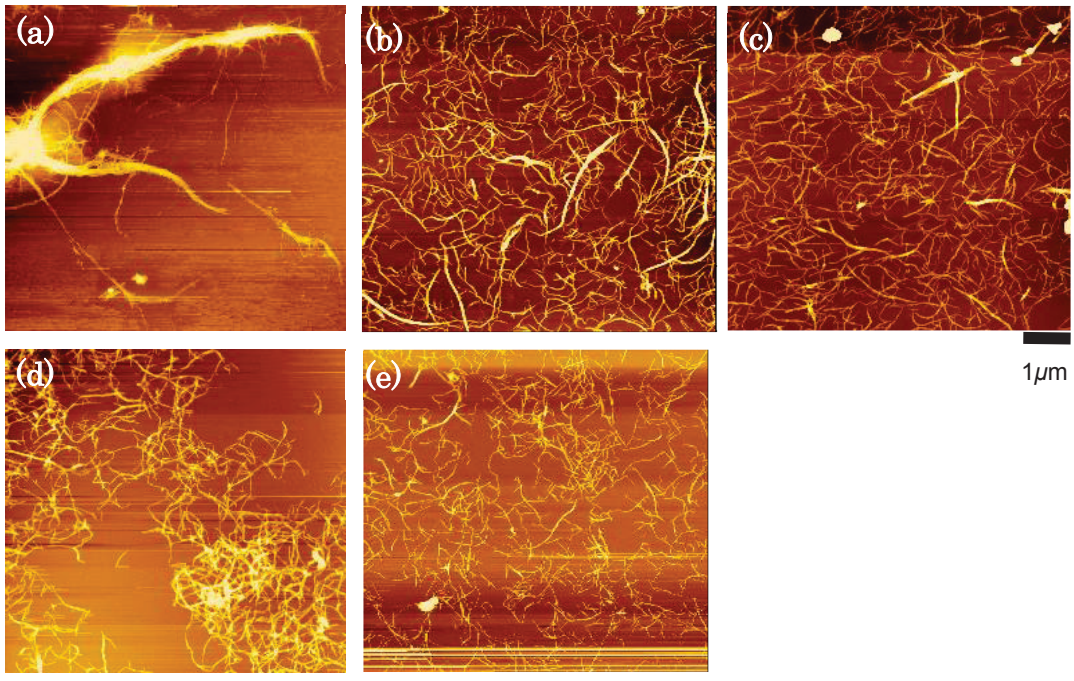


**Figure 13.** SPM images of *β*-chitin nanofibers after (a) 1, (b) 5, (c) 10, (d) 30 and (e) 50 passes treatments. The scale bar length is 1$\mu$m. Reproduced with permission from ref. 75. Copyright 2013, American Scientific Publishers.

**Table 3.** Width of *β*-chitin nanofibers.

| **Number of Passes** | 1 | 5 | 10 | 30 | 50 |
|---|---|---|---|---|---|
| **Fibers Width (nm)** | 13.2 | 6.0 | 5.1 | 4.7 | 3.8 |

### 2. 3. 2. Chemical and Crystalline Structures of Chitin Nanofibers

The FT-IR spectra were used to study the chemical structure of *β*-chitin nanofibers processed after 1, 5, 10, 30, and 50 passes by the HPWJ system. FT-IR spectra of the isolated nanofibers (data are not shown) were in good agreement with the spectrum of commercial *β*-chitin, for instance, the OH stretching band at 3431 $cm^{-1}$, the NH stretching band at 3265 $cm^{-1}$, the amide I band at 1652 and 1621 $cm^{-1}$, and the amide II band at 1554 $cm^{-1}$. This suggested that the chitin nanofibers had the original chemical structures of chitin even though high mechanical forces were applied during the treatments.

Wide-angle X-ray diffraction was used to examine the crystalline structure of the fibrillated nanofibers by the HPWJ system after several passes. The original squid pen and its nanofibers had major diffraction peaks at $2\theta = 9^{o}$ and $20^{o}$, which corresponds to the [020] and [110] planes, respectively. The peaks appeared at about the same reflection plane in each sample. Thus, the HPWJ system retains the original crystalline structure of *β*-chitin. Table 4 shows the degree of relative crystallinity of *β*-chitin powder and its nanofibers determined from X-ray diffraction profiles. The degree of the

relative crystallinity of the original *β*-chitin powder was 58.1%. However, there were no significant differences in the relative degree of crystallinity (57.8 - 57.4%), though 1 to 50 passes treatments straightly applied over the dispersions at the time of processing. This revealed that the crystallinity of chitin nanofibers was apparently independent on the number of mechanical treatments, as no damage of crystalline part occurred, even though a super-high-pressure water jet (240 MPa) was employed by the system. So the challenge of maintaining the natural crystallinity in nanofibers was successful, compared with other report.[54]

**Table 4.** Degree of relative crystallinity of *β*-chitin nanofibers.

| **Number of Passes** | Original | 1 | 5 | 10 | 30 | 50 |
|---|---|---|---|---|---|---|
| **Relative Crystallinity (%)** | 58.1 | 57.8 | 58.0 | 58.2 | 57.6 | 57.4 |

### 2. 3. 3. Transparency and Viscosity of Chitin Nanofiber Dispersions

The regular light transmittances of fibrillated chitin nanofibers slurry with 0.1 wt. % concentration at 400 nm wavelength are shown in Figure 14 graphed against the number of passes**.** Transparency is strongly associated with the thickness of chitin fibers, especially at shorter wavelength. As can be seen from the figure, squid pen *β*-chitin dispersed easily in water compared to *α*-chitin. That is, the suspension became transparent when the individualized nano-sized fibers dispersed in aqueous system. Different molecular chain packing, [37, 42] weak intermolecular forces, [44] and low degree

of crystallinity (Table 4) of $\beta$-chitin might be responsible for its dispersion behavior in water. At one pass, the light transmittance of $\beta$-chitin slurry was 73.4%. However, the transmittance steeply increased to 83.7%, at 5 passes. Finally, the transparency reached almost at its peak (86.99%) at 10 passes. These results suggested that, up until 10 passes, chitin fibers were fibrillated regularly into thinner nanofibers. Above 10 passes, on the other hand, distinct disintegration was almost impossible on increasing further cycles of treatments. Namely, remarkable fibrillation already accomplished, which lead to saturated transparency. These trends are in decent agreement with the results of SPM.

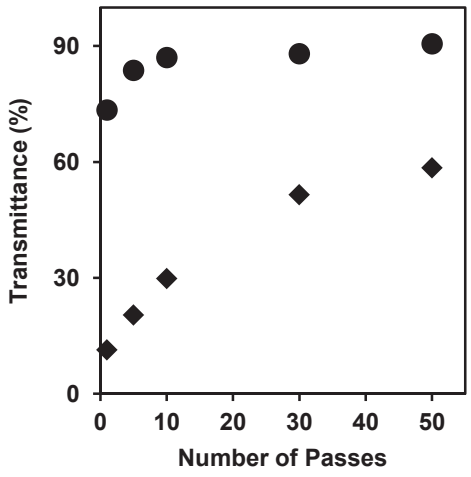


**Figure 14.** Regular light transmittances of $\alpha$-chitin nanofibers (diamond) and $\beta$-chitin nanofibers (circle) at 400 nm graphed against the number of passes. Reproduced with permission from ref. 75. Copyright 2013, American Scientific Publishers.

Figure 15 shows the viscosities of the chitin nanofiber slurry with 1.0 wt. %, fibrillated by the HPWJ system graphed against the number of passes. The viscosity of 1 pass $\beta$-chitin nanofibers slurry is 1560 cP. Though, the viscosity improved with

increasing the number of passes and reached to 3060 cP at 5 passes. In contrast, above 10 passes, the viscosity did not change cheekily up until 50 passes. Nanofibers morphology is brightly linked to viscosity, which in turns linked to fibers length and thickness. That is, the thinner and longer nanofibers are, and the more frequently they become entangled, which accelerate viscosity. The viscosity data indicated that, at around 5-10 passes, maximum entanglement of nanofibers occurred. Specifically, fibers with maximum length and considerable thickness are available within this part of analysis. Above 10 passes, the fibers length decreased, in addition to diameters, as the fibers started to break, and thereby lowering viscosity. These data are in excellent agreement with those obtained from the SPM images. On the other hand, $\alpha$-chitin nanofibrs viscosity was superior, due to the greater entanglement of nanofibers. Therefore, it was believed that the length of $\alpha$-chitin nanofibrs are greater than that of $\beta$-chitin nanofibers, which assessed from the SPM micrographs of both types of chitin nanofibers.

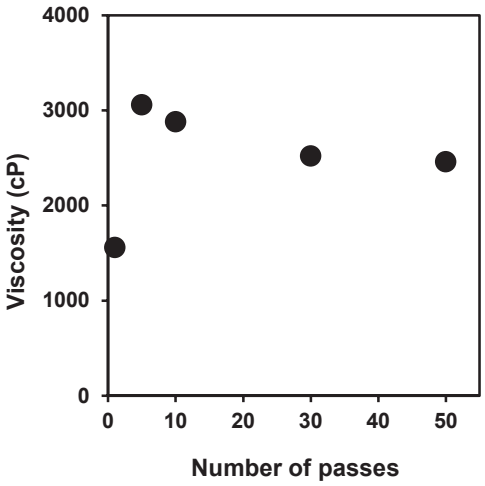


**Figure 15.** Viscosity of $\beta$-chitin nanofibers slurry graphed against the number of passes. Reproduced with permission from ref. 75. Copyright 2013, American Scientific Publishers.

### 2. 3. 4. Characterization of Chitin Nanofiber Sheets

Due to nano-size dimensions, chitin nanofibers were dispersed homogeneously in water and this unique property assisted to shape nanofibers into desired sheets by vacuum-filtration. The density of the chitin nanofiber sheets, in Figure 16, graphed against the number of passes. The sheet density of $\beta$-chitin nanofiber is 0.89 g $cm^{-3}$, at 1 pass, jumped to 0.95 g $cm^{-3}$ at 10 passes. Then again, above 10 passes, the value did not change meaningfully. However, Nanofibers morphology (shown in Fig. 13) and sheet density are correlated. The smaller and shorter $\beta$-chitin nanofibers can pack more easily than the $\alpha$-chitin nanofibers, which result relatively higher sheets densities of $\beta$-chitin.

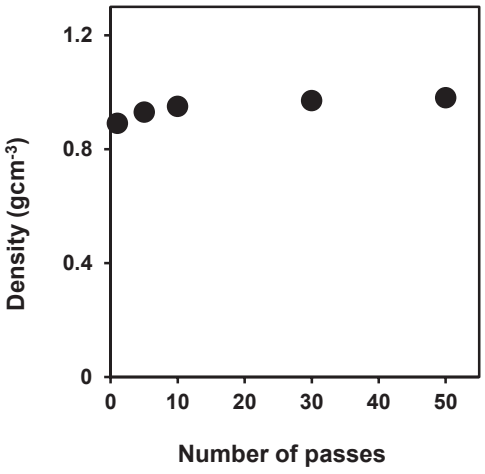


**Figure 16.** Density of $\beta$-chitin nanofiber sheets graphed against the number of passes. Reproduced with permission from ref. 75. Copyright 2013, American Scientific Publishers.

The Young's moduli and tensile strength of chitin nanofibers sheets are depicted in Figures 17 and 18, respectively, graphed against the number of passes. Young's moduli of $\beta$-chitin nanofiber sheets improved with increasing the number of treatments, and reached to a peak value of 2739.34 MPa at 5 passes than 1655.42 MPa at 1 pass. Moreover, the value did not change significantly following the further treatments from 10 to 50 passes. A similar trend for $\alpha$-chitin nanofiber sheets was noted earlier. On the other hand, tensile strength of chitin nanofiber sheets sharply increased from 28.39 MPa at 1 pass to 48.08 MPa at 5 passes. Later on, the values began to decrease abruptly from 10 passes (38.03 MPa) and finally, reached to the lowest value at 50 passes (19.68 MPa). These data completely deviated from the $\alpha$-chitin nanofiber sheets. In general, the mechanical properties of nanofiber sheets were found to be related with the aspect ratio (length: width) of fibers. Being, the nanofibers became thinner (Table 3) with the number of passes, the aspect ratio essentially increased up to some extent. That is, the

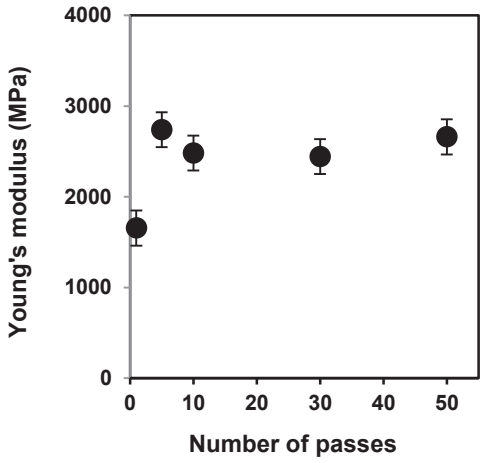


**Figure 17.** Young's moduli of $\beta$-chitin nanofibers graphed against the number of passes. Reproduced with permission from ref. 75. Copyright 2013, American Scientific Publishers.

longer and thinner nanofibers extended the number of hydrogen bonds between the fibers. In contrast, at higher passes, as mentioned earlier from the SPM images (Fig. 13), the fibers lengths shortened, which of course, dropped the aspect ratio of *β*-chitin nanofibers. In addition, the relative crystallinity of *β*-chitin is also low (Table 4). These could affect in a direct deterioration of the tensile property of chitin nanofiber sheets. It is beyond doubt that the mechanical properties are also affected by the sheet density.

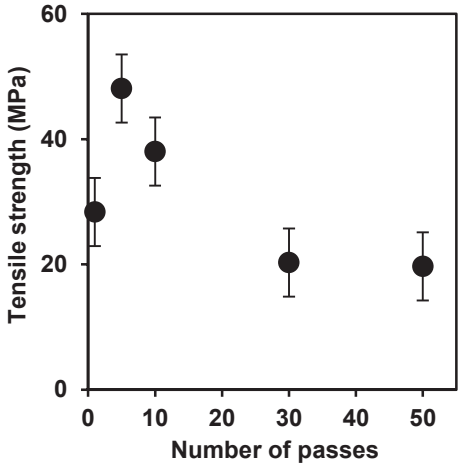


**Figure 18.** Tensile strength of *β*-chitin nanofibers graphed against the number of passes. Reproduced with permission from ref. 75. Copyright 2013, American Scientific Publishers.

Basically, Young's modulus and coefficient of thermal expansion (CTE) are anisotropic to each other. Young's modulus of a chitin nanofiber (not a sheet) estimated to be at least 150 GPa, whereas, its coefficient of thermal expansion (CTE) is very small.[36, 37] Table 5 shows the CTE values of *β*-chitin nanofiber sheets. The CTEs of all chitin nanofiber sheets, prepared from several passes, were less than 10 ppm $K^{-1}$. So, the

CTE did not change significantly after HPWJ treatments. This result also supports upholding of the characteristic extended crystalline structure of chitin nanofibers even after repeated fibrillation treatments.

**Table 5.** Coefficient of thermal expansion of *β*-chitin nanofiber sheets

| **Number of Passes** | 1 | 5 | 10 | 30 | 50 |
|---|---|---|---|---|---|
| **Thermal expansion (ppm $K^{-1}$)** | 9.17 | 8.06 | 8.65 | 7.87 | 9.48 |

## 2.4. Conclusion

Dry squid pen powder was transformed into nanofibers successfully by applying the HPWJ system. The morphology, chemical structure, crystallinity, viscosity, mechanical properties and thermal expansion of nanofibers was demonstrated elaborately. SPM images revealed that chitin nanofibers fibrillated to thinner fibers uniformly up to 10 passes. Light transmittances and viscosity of chitin nanofibers slurry also supported the SEM observations. Nanofibers with mean cross-sectional width of 3-4 nm were possible to isolate, although extensive cycles of treatment reduced the fibers lengths. The original *β*-chitin structure was maintained by the HPWJ system, in addition to the notable crystallinity of chitin nanofibers. The mechanical properties were improved by nano-fibrillation up to a particular range of treatments. These detailed characterizations are expected to play a vital role in developing commercial applications for the *β*-chitin nanofibers.

# Chapter 3

## Novel Preparation of Chitin Nanocrystals by $H_2SO_4$ and $H_3PO_4$ Hydrolysis

### 3.1. Introduction

Whiskers are very promising reinforcing materials for composites, owing to their high stiffness and strength.[57] These whiskers are almost free from defect and as a result, their properties are comparable to perfect crystals.[21] Inorganic nanofillers are mostly used to prepare nanocomposites with polymer matrices, although their processability, biocompatibility, and biodegradability are much more limited than those of naturally organic ones. However, increasing environmental awareness reflects the importance of using renewable raw materials for sustainable development. Polysaccharides are such natural gift with renewable, semi-crystalline properties to use as ideal nanofillers.

Chitin has been known to form microfibrillar arrangements, where the fibrils are tightly bound to each other through a large number of hydrogen bonds. These fibrils are typically embedded in a protein matrix and their diameters ranges from 2.5 to 2.8 nm depending on their biological origin.[58] Chitin microfibrils are consisted of alternative amorphous and crystalline domain. When chitin is subjected to strong acid treatment, disordered and low lateral ordered regions are hydrolyzed and dissolved, indicating water-insoluble, highly crystalline residues remain intact that have a higher resistance to

acid attack. These highly ordered nanocrystals have potentials to be used as highly functional materials.

Meanwhile, several groups isolated chitin nanocrystals (CNCs) from many chitins of different origins, such as squid pen[59], *Riftia* tubes[60], crab shells [58, 61 - 65], and shrimp shells [58, 66 - 71], using conventional hydrolysis in HCl solution (H-CNC). The final step of almost all types of nanocrystals preparation involved ultrasonic homogenization. The isolated nanocrystals had multiple aspect ratio and were studied as nanocomposite materials for reinforcement, as nanoscaffold in tissue engineering, and for other applications.[59 - 64, 71 - 73] Basically, the incorporation of CNCs to polymer matrices improved the thermomechanical properties of nanocomposites up to a certain extent. It is worth noting that the thermochemical behavior significantly depended on the crystalline nature of the CNCs, although most of the authors had no specific report on it. In addition, Sriupayo *et al*. reported that nanocomposites suffered thermal instability upon heat treatment.[68] Recently, Espinosa *et al*. isolated thermally stable cellulose nanocrystals by surface functionalization, through phosphoric acid hydrolysis, while the prepared nanocomposite remained transparent up to 180 $^{o}$C.[74]

In recent years, the author successfully prepared nanofibers from commercially available crab shell and squid pen chitin, respectively, using a novel high pressure water jet (HPWJ) system.[55, 75] This HPWJ treatment was advantageous over conventional technology in its atomization efficiency for preparing some bionanomaterials. In this study, the author made an attempt to prepare CNCs after hydrolyzing chitin powder through relatively stronger acids like $H_2SO_4$ (S-CNC) and $H_3PO_4$ (P-CNC), for the first

time. Initially, several reactions conditions were studied to find out a milder, suitable reaction environment for nanocrystals preparation. Special attentions were paid on CNC's morphology, dimensions and crystallinity. Besides, the chemical structure, percentage yield, water dispersibility, and the transparency of all types of CNCs were studied and compared. Finally, the unique thermal stability of P-CNCs in comparison with the native H- and S-CNCs was stated.

## 3. 2. Experimental

### 3. 2. 1. Materials

Chitin powder from crab shell was received from Koyo Chemical (product name: Chitin TC-L) and used without further purification. Hydrochloric acid from Kanto Reagent, and sulfuric and phosphoric acids from Wako Pure Chemical Industries, were commercial products and used as received.

### 3. 2. 2. Preparation of Chitin Nanocrystals

H-, S-, and P-CNCs were prepared by the acid hydrolysis of chitin powder using HCl, $H_2SO_4$, and $H_3PO_4$, respectively. With a slight modification, the conventional method of Paillet *et al*. was used to prepare H-CNCs by HCl hydrolysis.[59] In brief, chitin powder (5 g) was treated in 3 N HCl (100 mL) under vigorous stirring, at 100 $^oC$ for 90 min. After the acid hydrolysis, the suspension was immediately diluted with cold

deionized water to stop reaction, followed by centrifugation at 10,000 rpm to separate the obtained chitin solid fraction from the soluble fraction in water. This process was repeated several times until the supernatant appeared turbid and could no longer be decanted without significant product loss. The suspension was dialyzed against a large excess of deionized water until the pH of the suspension stabilized to 7. Following the removal of excess acid, the suspension was dispersed by ultrasonic homogenizer just for one minute. The suspension can disperse homogeneously, owing to the presence of slight positive charges on surfaces by the protonation of the amino group.[58] Finally, the dispersion was passed through the HPWJ homogenizer (Star Burst Mini, HJP-25001S, Sugino Machine) equipped with a ball-collision chamber. The slurry was ejected from a small nozzle with a diameter of 100 $\mu$m under high pressure of 245 MPa and collided with a ceramic ball with a diameter of 12.7 mm. Ten cycles of treatments were executed throughout the suspension. However, the author deliberately followed the above stated procedures for the isolation of S-CNCs and P-CNCs. Tables 6 and 7 summarize the conditions and results of the $H_2SO_4$ and $H_3PO_4$ hydrolysis treatments of chitin powder.

### 3. 2. 3 Characterization

The elemental analysis (EA) data obtained using an elemental analyzer (Elementar Vario EL Ⅲ, Elementar). The degrees of substitution (DS) of the sulfonic acid groups were calculated by comparing the weight percent of N and S atoms from EA data.

**Table 6.** Sulfuric acid hydrolysis of chitin to prepare chitin nanocrystals (S-CNC)

| Samples | Hydrolysis Conditions | | | Results | | |
|---|---|---|---|---|---|---|
| | 95% $H_2SO_4$ (mL) | Temperature ($^oC$) | Time (min) | Shapes [a] | % Yield | $DS_{SO3H}$ [b] |
| **S1-CNC** | 15 | 50 | 90 | Nanocrystals | 83 | 0 |
| **S2-CNC** | 15 | 50 | 60 | Nanofibers | 83 | 0.16 |
| **S3-CNC** | 20 | 50 | 60 | Long Nanocrystals | 83 | 0.86 |
| **S4-CNC** | 25 | 50 | 90 | Short Nanocrystals | 80 | 0 |

[a]Determined from SPM images
[b]Determined from elemental analysis data

**Table 7.** Phosphoric acid hydrolysis of chitin to prepare chitin nanocrystals (P-CNC)

| Samples | Hydrolysis Conditions | | | Results | |
|---|---|---|---|---|---|
| | 85% $H_3PO_4$ (mL) | Temperature ($^oC$) | Time (min) | Shapes [a] | % Yield |
| **P1-CNC** | 30 | 80 | 90 | Nano- crystals and fibers | 83 |
| **P2-CNC** | 50 | 80 | 90 | Nanocrystals | 80 |
| **P3-CNC** | 50 | 80 | 60 | Thick Nanocrystals | 82 |

[a]Determined from SPM images

Infrared spectra of the samples were recorded with an FT-IR spectrophotometer (Spectrum 65, Perkin-Elmer Japan) equipped with an ATR attachment.

A scanning probe microscopic (SPM) apparatus (Seiko Instruments) were used to record the SPM micrographs. Samples for SPM measurements were prepared by applying one drop of an aqueous CNC dispersion (0.1 mg $mL^{-1}$) on a freshly cleaved mica round disk followed by oven drying. Images were recorded as 256 × 256 pixel images for a 5 $\mu$m wide square. SPM images were used to measure the widths of CNCs by selecting the measuring points along the fiber axes. Such measurements were made for more than 50 points on isolated nanofibers in each image.

X-ray diffraction profiles of the dried nanocrystals were obtained with Ni-filtered CuK$\alpha$ from an X-ray generator (Ultima IV, Rigaku) operating at 40 kV and 30 mA. The diffraction profile was detected using X-ray goniometer scanning from $5^{o}$ to $35^{o}$. The crystalline index (CI) was determined by following the equation: $CI = (I_{110} - I_{am}) \times 100/I_{110}$, where $I_{110}$ is the maximum intensity of the [110] plane and $I_{am}$ is the intensity of the amorphous diffraction at $16^{o}$.[35]

The light transmittances of individual dispersions were measured using a UV-Vis spectrophotometer (V550; JASCO). An ultrasonic homogenizer was used to prepare 0.1 wt. % dispersion of CNCs in water for UV-Vis measurement.

The thermal stability of CNCs was studied on a TG/DTA6300 (Seiko Instruments). The sample was approximately 5 mg and heated in argon at a rate of 10 $^{o}$C

$min^{-1}$ up to 500 $^{o}$C. To calculate the percentage yield of each CNC, samples were dried by permitting a slow evaporation at 50 $^{o}$C before the ultrasonic homogenization step of isolation.

## 3. 3. Results and Discussion

### 3. 3. 1. Morphology and Size of Chitin Nanocrystals

SPM micrographs of H-, S-, and P-CNCs are depicted in Figures 19, 20 and 21, respectively, which show the morphology of the CNCs on acid hydrolysis and subsequent high-pressure water jet treatments under diverse reaction conditions. Figure 19 displays the H-CNC fragments consisting of both individual and aggregate nanocrystals. The chitin fragments consisting of slender rods with sharp ends were broadly distributed. The average thickness of H-CNCs was found to be 9.3 nm, as measured from the SPM image. On the other hand, although the morphology of S-CNCs [(Fig. 20 (a)-(d)) and P-CNCs (Fig. 21(a)-(c)] depended on the hydrolysis conditions i.e., the chitin-to-acid ratios, as well as hydrolysis time (Tables 6 and 7), basically the hydrolysis was completed without aggregation. These nano-chitins were separated as short, long, thick nanocrystals and nanofibers, depending on their length and width. The reaction conditions influenced the length, thickness, and uniformity of S-CNCs, clarified from the SPM images in Figure 20. For instance, individualized nanocrystals of uniform shapes and sharp end, produced when hydrolyzed at an ideal state (Fig. 20(c)). At this stage, the reaction conditions were enough not only to produce homogeneous CNCs, but also to improve surface functionalities. Besides, the change of

hydrolysis time made interesting results, such as, fiber shaped nanocrystals i.e. nanofibers formed rather than rod like crystals (Fig. 20 (b)). The average cross-sectional width of S-CNCs measured 8 nm, from a particular SPM image (Fig. 20 (c)). On the contrary, Figure 21(a) showed the formation of mixtures of particles, i.e., fiber and rod like shaped nanocrystals of different sizes, upon hydrolysis by $H_3PO_4$. Even though, just after changing the chitin-to-acid ratio, individualized sharp rod-like chitin fragments with homogeneous distribution were found (Fig. 21(b)) over a large area. On the other hand, the short hydrolysis time didn't make any major change in the morphology of P-CNCs (Fig. 21(c)), although thick nanocrystals appeared. In this occasion, the average cross-sectional widths of P-CNCs were found to be 7.3 nm, measured from a respective SPM image (Fig. 21(b)).

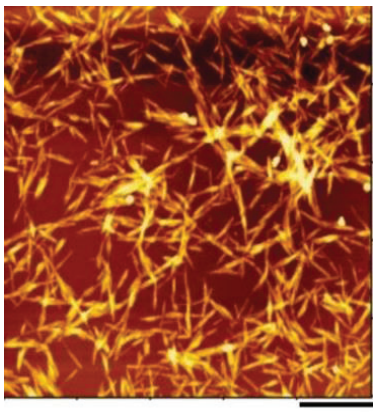

**Figure 19.** SPM image of H-CNC. The scale bar length is 1 $\mu$m. Reproduced with permission from ref. 80. Copyright 2013, American Scientific Publishers.

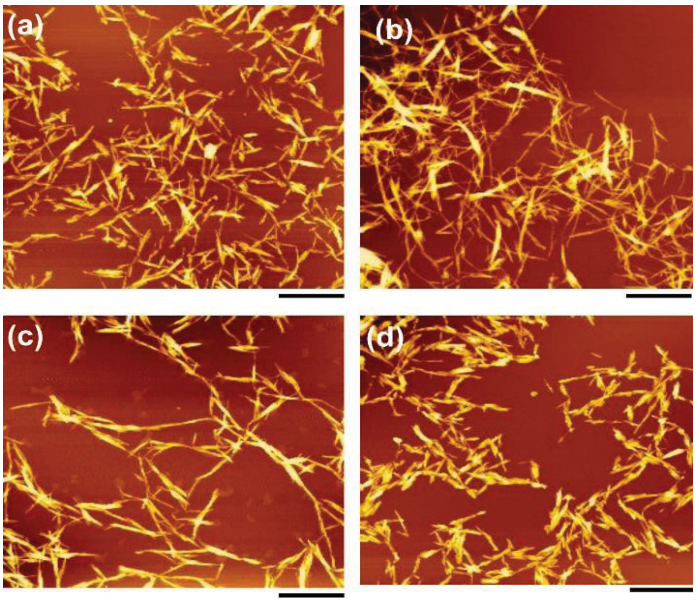


**Figure 20.** SPM images of (a) S1-, (b) S2-, (c) S3-, and (d) S4-CNC. The scale bar length is 1$\mu$m. Reproduced with permission from ref. 80. Copyright 2013, American Scientific Publishers.

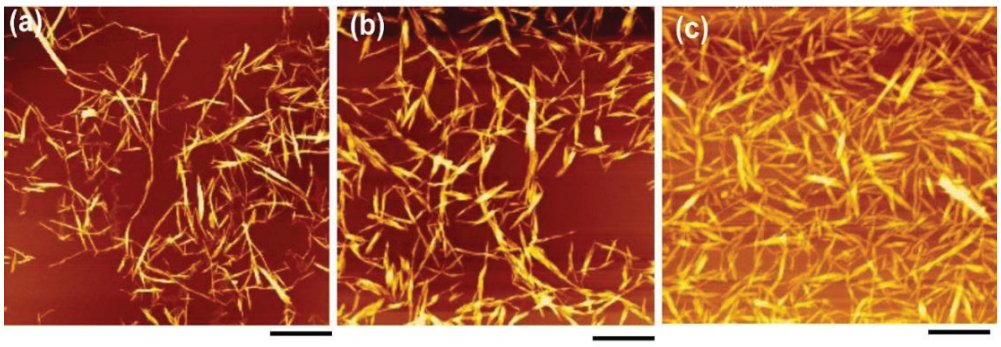


**Figure 21.** SPM images of (a) P1-, (b) P2-, and (c) P3-CNC. The scale bar lengths are 1$\mu$m. Reproduced with permission from ref. 80. Copyright 2013, American Scientific Publishers.

### 3. 3. 2 Chemical Structures of Chitin Nanocrystals

The FT-IR spectra were used to evaluate the chemical structures of all kinds of CNCs after being processed by acid hydrolysis and subsequent high-pressure water jet treatment. All spectra of CNCs from distinct sources were in good agreement with the spectrum of the commercial chitin (data are not shown). The OH stretching band at 3431 $cm^{-1}$, the NH stretching band at 3265 $cm^{-1}$, the amide I bands at 1652 and 1621 $cm^{-1}$, and the amide II band at 1554 $cm^{-1}$ of the chitin nanocrystal are characteristic of chitin. Although S-CNC has a slight sulfate group on the surface (Table 6), no other additional peaks were observed. Moreover, the high-pressure water jet system does not affect the chemical structures of chitin nanofibers, as we reported earlier.

### 3. 3. 3 Crystalline Structures of Chitin Nanocrystals

Wide-angle X-ray diffraction (WAXD) was used to examine the crystalline structures of the isolated CNCs by respective acid hydrolysis. Figure 22 represents the WAXD patterns of CNCs of separate sources, at $2\theta$ = 9.2, 19.1, 20.9, and 23.1°, corresponding to [020], [110], [120], and [130] planes, respectively. These reflection planes are typical antiparallel crystal patterns of $\alpha$-chitin.[37] Thus, an intractable crystalline structure of chitin was sustained even after successive acid hydrolysis and water jet treatments. Table 8 shows the degree of relative crystallinity of $\alpha$-chitin powder and its nanocrystals determined from X-ray diffraction profiles. The degree of relative crystallinity of the original α-chitin powder is 83.7%.[55] However, significant decrease in relative crystallinity was observed in the case of H-CNCs (70.0%). In our

knowledge, there has been no specific report on relative crystallinity of CNCs derived from crab shell by acid hydrolysis. Although, Morin and Godrich *et al.*, reported the maximum crystallinity of whiskers from *Riftia* tubes 58% and from shrimp shells 84%, respectively.[60, 68] A possible explanation is that during the processing of H-CNCs, some parts of the crystallite were converted into amorphous chitin, although acid hydrolysis was faster in the amorphous region than in the crystalline region. Moreover, amorphous chitin is more hydrophobic, which assisted dried samples of nanocrystals to absorb moisture. In contrast, the degrees of relative crystallinity of isolated S-CNCs ranged from 86 to 93.4% and of P-CNCs from 89 to 92.6%, depending on various reaction conditions. We speculate that HCl treatment at 100 $^{o}$C collapsed crystalline part of chitin resulted in reducing relative crystallinity. On the other hand, strong acid treatments using $H_2SO_4$ and $H_3PO_4$ under milder temperature hydrolyzed amorphous part resulted in higher relative crystallinity.

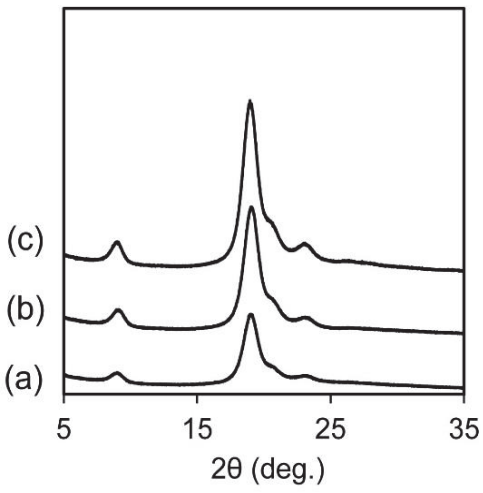


**Figure 22.** X-ray diffraction profiles of (a) H-, (b) S3-, and (c) P2-CNCs. Reproduced with permission from ref. 80. Copyright 2013, American Scientific Publishers.

**Table 8.** Degree of relative crystallinity of chitin nanocrystals

| **Samples** | Chitin | H-CNC | S3-CNC | P2-CNC |
|---|---|---|---|---|
| **Relative Crystallinity (%)** | 83.7 | 70.0 | 93.4 | 92.6 |

### 3. 3. 4. Percentage Yield, Dispersibility and Transparency of Chitin Nanocrystals

The yield of H-CNC on calculation found 87%, while that of S- and P-CNC found in the range of 80-83%. It is interesting to note that the hydrolysis of chitin powder by $H_2SO_4$ and $H_3PO_4$ produced very similar results, although various reaction conditions applied during the synthesis. The possibility is that both types of hydrolysis could dissolve almost the similar amount of amorphous parts from the chitin powder. The percentage of relative crystallinity of S- and P-CNC revealed the similar effects. On the other hand, the acid treatment of chitin powder by HCl failed to dissolve the same amount of amorphous chitin like its counterparts. It is beyond doubt that small amount of process loss occurred during the course of isolation processes of CNCs.

All types of CNC dispersions of 0.1 wt. % were made to investigate their water dispersibility and transparency. As can be seen from Figure 23, chitin nanocrystals homogeneously dispersed in water and formed a stable suspension. The dispersibility of nanocrystals depends strongly on their aspect ratio, surface functionalization, and the ability of the solvent and the surface groups to counterbalance the attractive hydrogen-bond interactions exerted by the abundant hydroxyl groups. H-CNCs

displayed better dispersibility with their corresponding S-CNCs and P-CNCs in water. Since amorphous chitin is more hydrophilic than chitin crystal, H-CNC with lower crystallinity has higher dispersibility than S- and P-CNC. However, all of the CNC dispersions remained stable for almost a month, without phase separation. The stability is attributable to the frequent electrostatic repulsions between the chitin nanoparticles in water.

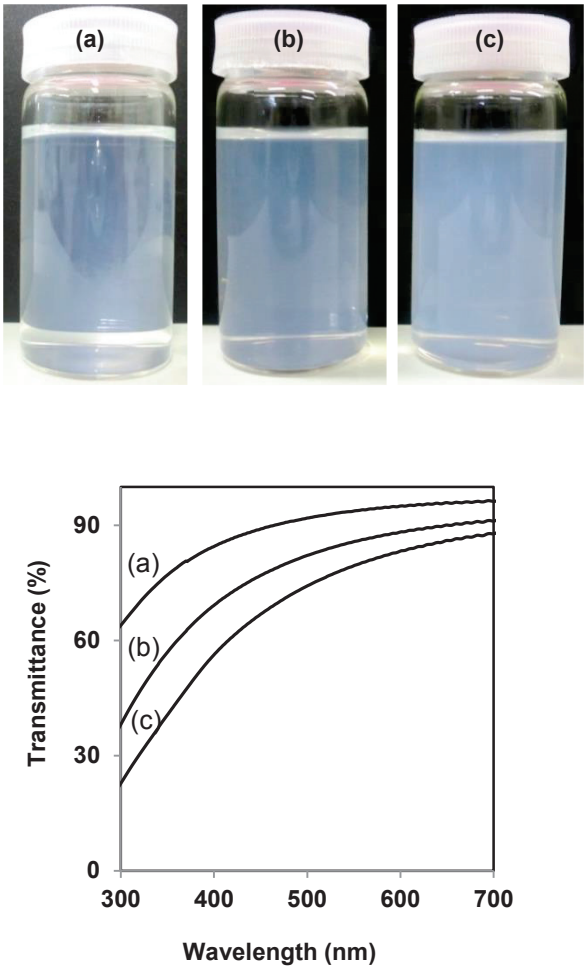


**Figure 23.** Digital images and UV-Vis transmittances of (a) H-, (b) S3-, and (c) P2-CNC dispersions with 0.1 wt. % concentration. Reproduced with permission from ref. 80. Copyright 2013, American Scientific Publishers.

### 3. 3. 5. Thermal Stability of Chitin Nanocrystals

Thermogravimetric analysis (TGA) of CNCs isolated through various hydrolysis conditions was carried out to evaluate their degradation profiles and thermal stability. Figure 24 represents TGA and derivatives of TGA curves of P-CNC, S-CNC, and H-CNC between 150 and 500 $^{o}$C. After drying, P-CNC displays the highest thermal stability with only one weight-loss step. Moreover, H-CNCs and S-CNCs present an almost identical two-step weight loss behavior, with the main difference occurring in the temperature range of 300-400 $^{o}$C. According to the derivatives of the TGA curves, H-CNC and S-CNC each have two kinds of thermal decomposition acts. In the case of H-CNC, a major degradation peak is at 378.5 $^{o}$C, while a minor degradation peak is at approximately 285 $^{o}$C. On the other hand, S-CNC shows two degradation behaviors at about 325 and 392 $^{o}$C, respectively. In contrast, the derivative curve of TGA of P-CNC

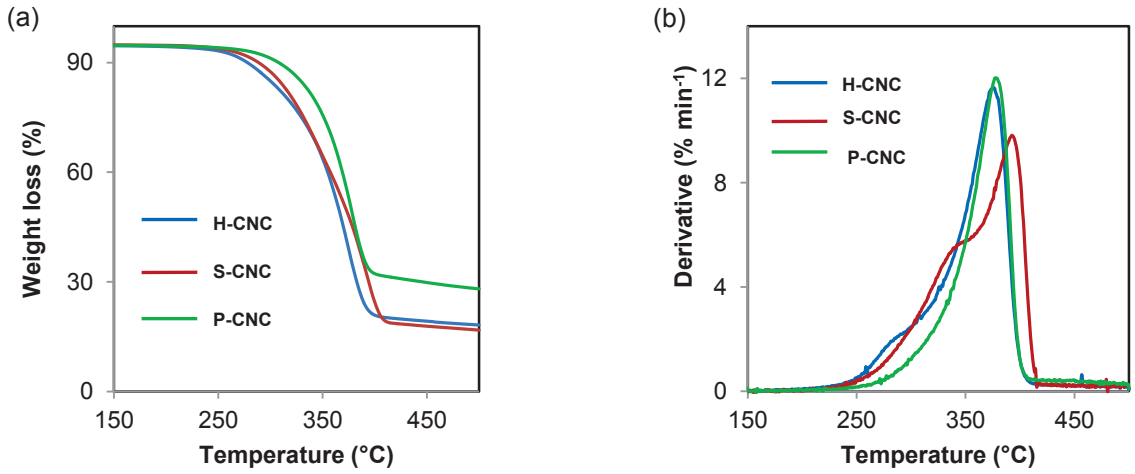


**Figure 24.** (a) TGA and (b) derivative of TGA curves of H-, S-3, and P2-CNCs in Argon. Reproduced with permission from ref. 80. Copyright 2013, American Scientific Publishers.

displays a single sharp degradation step at 378.5 $^{o}$C. The higher thermal stability is due to the high relative crystallinity of P-CNC.

## 3. 4.Conclusion

$H_2SO_4$ and $H_3PO_4$ were used to hydrolyze chitin powder to prepare CNCs. After examining the results of SPM, the influences of hydrolysis conditions on the CNCs' morphology were discussed. Irrespective of the nature of acids and reaction conditions, a high yield of CNCs was achieved. The average thickness of CNCs ranged from 7.3 to 8.0 nm. However, S- and P-CNCs showed higher crystallinity than the conventional H-CNCs. The represented hydrolysis conditions might be suitable for preparing highly crystalline CNC. Moreover, TGA results showed P-CNCs have higher thermal stability than H- and S-CNCs. All types of CNCs formed stable dispersions in water and had high transparency. Thermally stable P-CNC prepared by a lower reaction temperature and with lower acid volume might be appropriate as filler in the design of polymer nanocomposites, together with some other applications. Thus, HPWJ technology emerged as a powerful disintegration tool for preparing nanomaterials.

# Chapter 4

## Simple Preparation of Chitosan Nanofibers by Using High Pressure Water Jet System

### 4.1. Introduction

Chitosan is a linear $\beta$-(1-4)-linked cationic polysaccharide composed of randomly distributed glucosamine and *N*-acetylglucosamine units. It is derived from partial deacetylation of chitin, which is the main component of exoskeletons of crustaceans and mollusks. This polymer naturally is honored with biocompatibility and biodegradability along with cellular-binding, wound-healing, anti-bacterial, and anti-fungal properties. Therefore, chitosan has been considered with great potential in many applications including food, cosmetic, biomedical, water processing, and biofilm formation.[14 - 17, 19]

The electrospinning process enables the artificial production of nanofibers from a wide range of natural polymer solutions using interactions between fluid dynamics, electrically charged surfaces, and electrically charged liquids.[23, 76, 77] However, electrospinning of chitosan itself is difficult due to its polycationic nature. The cationic charge increases the excessive surface tension of the solution,[20] meaning that a higher electrical force is required for nanofiber production. Another synthetic polymer is therefore usually mixed with chitosan to improve its electrospinnability.[78, 79]

In the meantime, the author successively synthesized chitin nanofibers (both $\alpha$- and $\beta$-type), as well as chitin nanocrystals from the commercially available chitin powder, effectively.[55, 75, 80] Since the chitin powder is made up of regularly structured chitin nanofibrill aggregates, it was possible to downsize nanofibers using a very simple high pressure water jet (HPWJ) disintegration system. The chitin nanofibers obtained from the commercial sources had highly uniform network morphology of 4-6 nm in width.[56] In this study, the author describes the nano-fibrillation of chitosan with 1-50 passes of the HPWJ system in water. The nanofibers at the same time have characterized with their morphology, transparency, viscosity, mechanical properties, and thermal expansion. Although, the electrospinning process is a "bottom-up" approach as it bundles molecules into fibers, the HPWJ process is considered to be a "top-down" approach. Utilizing the HPWJ system to create these nanofibers has several advantages over the electrospinning approach, including its low energy costs, high-volume production, organic solvent-free system, and excellent formability.[34]

## 4. 2. Experimental

### 4. 2. 1. Materials

Chitosan powder (cat. no. C0831, Mw: 420,000, degree of deacetylation: 78%) was purchased from Tokyo Chemical Industry and washed with water by filtration prior to use.

### 4. 2. 2. Preparation of Chitosan Nanofibers

Chitosan nanofibers were prepared followed by the similar procedure stated in our previous articles.[55] Purified chitosan powder was dispersed in water at 1 wt. %. The dispersion was roughly crushed with a grinder and then passed through the HPWJ system (Star Burst Mini, HJP- 25001S, Sugino Machine Co., Ltd.) equipped with a ball-collision chamber. The slurry was ejected from a small nozzle with a diameter of 100 $\mu$m under high pressure of 245 MPa and collided with a ceramic ball with a diameter of 12.7 mm. The suspension was passed through 1, 5, 10, 30, and 50 mechanical treatments, periodically.

### 4. 2. 3. Preparation of Chitosan Nanofibers Sheets

Fibrillated chitosan nanofibers were dispersed in neutral water at a fiber content of 0.1 wt. %. The suspension was stirred under reduced pressure and vacuum-filtered using a membrane filter. The obtained chitosan nanofibers sheets were dried at 100 $^{o}$C, in a hot-press for 30 minutes. The dried sheets were cut into 5 cm × 5 cm squares with an approximate thickness of 29 $\mu$m and a weight of approximately 70 mg.

### 4. 2. 4 Characterization

Infrared spectra of the samples were performed with an FT-IR spectrophotometer (Spectrum 65, Perkin-Elmer Japan Co., Ltd.,) equipped with an ATR attachment.

Chitosan nanofibers cast film was prepared for field emission scanning electron microscopic (FE-SEM) observation. The prepared nanofibrs suspension was dried in an oven, after replacing water with EtOH. The film was coated with an approximately 2 nm layer of Pt by an ion sputter coater and observed by FE-SEM (JSM-6700F; JEOL, Ltd.) operating at 2.0 kV.

X-ray diffraction profiles of the nanofibers were recorded with Ni-filtered CuK$\alpha$ from an X-ray generator (Ultima IV, Rigaku) operating at 40 kV and 30 mA. The diffraction profile was detected using X-ray goniometer scanning from $5^{o}$ to $35^{o}$. The crystalline index (CI) was evaluated by following the equation: $CI = (I_{110} - I_{am}) \times 100/I_{110}$, where $I_{110}$ is the maximum intensity of the [110] plane and $I_{am}$ is the intensity of the amorphous diffraction at $16^{o}$.[35]

The regular luminous transmittances of chitosan nanofibers suspensions were determined at wavelengths form 200 to 900 nm using a UV-Vis spectrophotometer (V550; JASCO, Tokyo, Japan).

Viscosity was performed by conducting a Brookfield digital viscometer DV-E, using spindle no. LV-4 (Brookfield Engineering Laboratories, Middleboro, MA).

The Young's modulus and tensile strength analysis of sheets were measured using a universal testing instrument (AG-X, Shimadzu, Tokyo, Japan) for samples 50 mm long and 10 mm wide. At least five specimens were tested for their nanofibers sheets.

The coefficients of thermal expansion (CTE) of the sheets were obtained with a thermomechanical analyzer (Q400, TA Instruments, Newcastle, DE). Specimens were 30 mm long and 3 mm wide, with a 20 mm span. The measurements were carried out three times during elongation from 30 $^{o}$C to 165 $^{o}$C by elevating the temperature at a rate of 5 $^{o}$C min$^{-1}$ in a nitrogen atmosphere in tensile mode under a load of 0.05 N. The CTE values were determined in the second run in order to dry the sample completely in the first run.

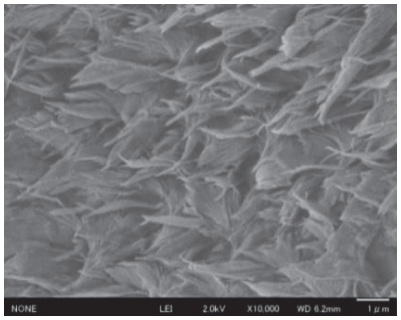


**Figure 25.** FE-SEM micrograph of chitosan flakes. Reproduced with permission from ref. 90. Copyright 2013, Elsevier.

## 4. 3. Results and Discussion

### 4. 3. 1. Morphological Observations of Chitosan Nanofibers

It is known that crab shell is made up of an aggregation of chitin nanofibers. Figure 25 shows a surface image of the chitosan powder used in this study.

Characteristic fibrous morphology was observed after deacetylation, suggesting that nanofibers may be obtained from chitosan powder after breaking down its structure. Figure 26 shows the FE-SEM micrographs of a chitosan after HPWJ treatment with 0, 1, 5, 10, 30, and 50 passes in distilled water. In Figure 26(a), shows that the chitosan powder has been roughly crushed by a grinder, has a fibrous structure. The thick aggregate of fibrous chitosan was broken down further into a mixture of micro- and nano-sized fibers after only one pass of the HPWJ treatment (Fig. 26(b)). After 5 passes, the fiber width decreased further due to fibrillation of the micron-sized fibers (Fig. 26(c)), although a small number of fibers approximately 100 nm in width remained. After 10 passes, most of the chitosan aggregate was well-fibrillated into fibers on the scale of tens-of- nanometers and had a very fine nanofiber network. Further mechanical treatments resulted in no significant changes in nanofiber formation, although the average fiber diameters decreased to some extent, from 40.8 nm (10 passes) to 36.6 nm (30 passes) and 34.8 nm (50 passes). In conclusion, the nanofiber morphology correlated strongly with the number of passes up until 10 passes. This result indicates that the chitin nanofiber aggregate structure was still maintained after deacetylation of chitin, which allows nano-fibrillation of chitosan powder. In contrast, we found that chitosan nanofibers could not be obtained from regenerated chitosan prepared by regeneration from chitosan solution in aqueous acetic acid.

### 4. 3. 2. Chemical and Crystalline Structures of Chitosan Nanofibers

The FT-IR spectra were used to evaluate chemical structure of chitosan fibers processed after 0, 1, 5, 10, 30, and 50 passes by the HPWJ system. Chitosan nanofibers

exhibited a number of absorbance peaks assigned to OH stretching band at 3445 $cm^{-1}$ overlapped with NH stretching band, the CH stretching bend at 2872 $cm^{-1}$, the amide I band at 1652 and 1621 $cm^{-1}$, and the amide II band at 1554 $cm^{-1}$. All spectra of the obtained nanofibers were in excellent agreement with the spectrum of commercial chitosan (data are not shown). This suggests that the HPWJ system retain the original chemical structures of chitosan even with 50 passes treatment.

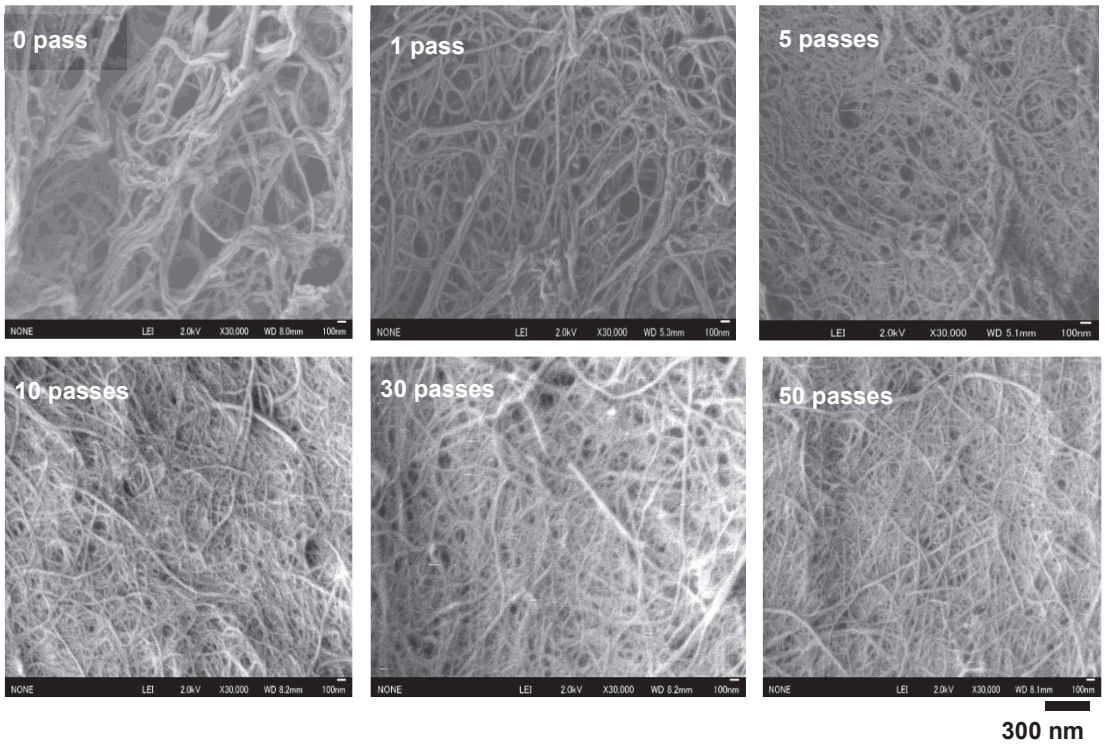


**Figure 26.** SEM images of chitosan nanofibers after several passes treatments by HPWJ system. The scale bar length is 300 nm. Reproduced with permission from ref. 90. Copyright 2013, Elsevier.

Wide-angle X-ray diffraction is the principal process that has been used to examine the crystalline structure of the fibrillated nanofibers by the HPWJ system after several passes. All chitosan samples showed major reflection at $2\theta = 9^{o}$ and 20◦, which corresponds to [020] and [110] reflections, respectively.[37] The peaks appeared at about the same reflection plane in each sample. Figure 27 represents the relative degrees of crystallinity of chitosan nanofibers determined from the X-ray diffraction profiles. It was found that the relative degree of crystallinity decreased linearly from 48.1% (0 pass) to 39.5% (50 passes) after the HPWJ processes. These results indicate that HPWJ treatments damage the crystalline part of the chitosan fibers, likely due to the system employing a super high-pressure water jet of 245 MPa. The crystallinity of chitosan is considerably lower than that of chitin.[34]

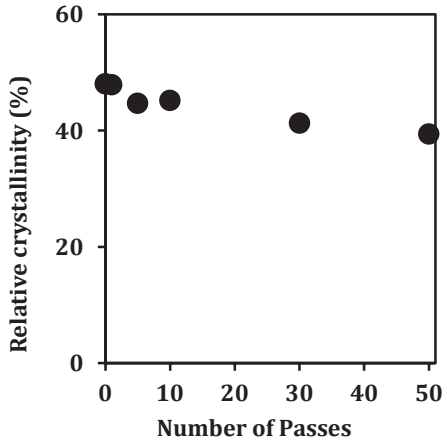


**Figure 27.** Degree of relative crystallinity of chitosan nanofibers as a function of number of passes. Reproduced with permission from ref. 90. Copyright 2013, Elsevier.

### 4. 3. 3. Transparency and Viscosity of Chitosan Nanofiber Suspensions

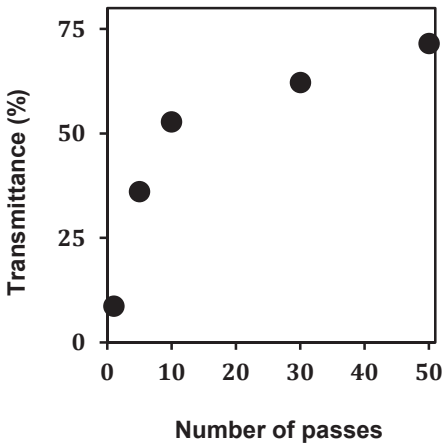


**Figure 28.** Regular light transmittance of chitosan nanofiber suspensions at 600 nm graphed against the number of passes. Reproduced with permission from ref. 90. Copyright 2013, Elsevier.

The regular light transmittances of fibrillated chitosan nanofibers slurry with a 0.1 wt. % concentration at 600 nm wavelength are shown in Figure 28 graphed against the number of passes. Since transparency is strongly associated with the chitosan fiber thickness, we can see the morphological change of chitosan nanofibers after HPWJ treatments from the data.[49] That is, when solid fibers were dispersed at the nano level, the suspension became transparent. At 0 passes, the chitosan was not dispersed, but precipitated in water. At 1-10 passes, the light transmittance of the chitosan slurry increased steeply from 8.6 to 52.8%, respectively. Above 10 passes, the increase in transmittance became more gradual; these results suggest that up until 10 passes the chitosan fibers were fibrillated regularly into thinner nanofibers. Above 10 passes, however, the chitosan was so fibrillated that it was difficult to achieve significant

disintegration in response to further passes, resulting in a saturated transparency. These trends agree well with the FE-SEM observations. After the HPWJ treatment, chitosan nanofibers were dispersed homogeneously in water for at least 1 month, although conventional chitosan powder precipitated in water immediately. Chitosan nanofibers can therefore be easily mixed with other products and shaped into the desired forms.

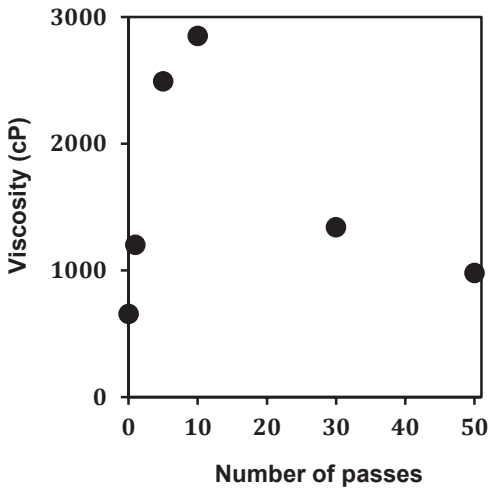


**Figure 29.** Viscosity of chitosan nanofiber suspensions as a function of number of passes. Reproduced with permission from ref. 90. Copyright 2013, Elsevier.

Figure 29, illustrates the viscosities of the chitosan nanofiber slurries with 1.0 wt. % fibrillated by the HPWJ system as a function of number of passes from 0 to 50. The viscosity of zero pass chitosan nanofibers is 657 cP. However, the viscosity improved with increasing the number of passes and reached to 2850 cP at 10 passes. On the other hand, above 10 passes, the viscosity decreased abruptly to 980 cP at 50 passes. Nanofibers morphology is brightly linked to viscosity. Moreover, nanofibers entanglements have a close relationship with the fibers length and diameters. That is,

the thinner and shorter chitosan nanofibers are, and the more frequently they become entangled, which rises viscosity. The viscosity data indicated that, up to around 10-30 passes, the nanofiebrs became thinner as the number of passes increased. Above which the nanofibrillation was remarkably ended, while the fibers length decreased, in addition to diameters, as the fibers started to break, thereby lowering viscosity. These results are in good agreement with those obtained from the FE-SEM images.

### 4. 3. 4. Characterization of Chitosan Nanofibers Sheet

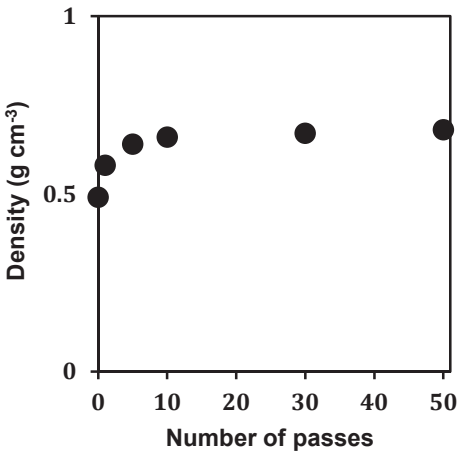


**Figure 30.** Density of chitosan nanofiber sheets as a function of number of passes. Reproduced with permission from ref. 90. Copyright 2013, Elsevier.

Since the chitosan nanofibers were homogeneously dispersed in water, nanofiber sheets were easily prepared by vacuum filtration. Figure 30 represents the density of the chitosan nanofiber sheets as a function of the number of passes. The density sharply increases from 0.49 to 0.66 g $cm^{-3}$ at 0-10 passes, respectively. After 10 passes, the value seems saturated. The sheet density is associated with the chitosan nanofiber

morphology. That is, the thinner the chitosan nanofibers, the more densely the nanofibers are packed in the sheet.

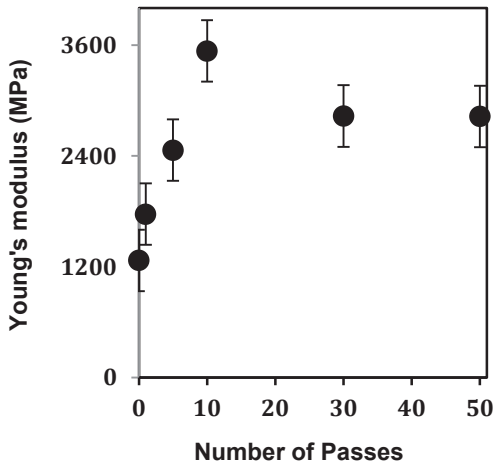


**Figure 31.** Yong's moduli of chitosan nanofiber sheets graphed against the number of passes. Reproduced with permission from ref. 90. Copyright 2013, Elsevier.

Figures 31and 32 display the Young's moduli and tensile strengths of the chitosan nanofiber sheets graphed against the number of passes, respectively. Both Young's moduli and the fracture strengths of the chitosan nanofiber sheets increase with increases in the number of passes, reaching their peaks at 10 passes at 3535 MPa and 59.9 MPa, respectively. These values begin to decrease gradually above 10 passes, reaching 2828 MPa and 36.1 MPa, respectively, at 50 passes. In general, the mechanical properties of the nanofiber sheets were found to be related to the nanofiber width. When the chitins were fibrillated into a number of nanofibers, the chance of hydrogen-bonding interactions between nanofibers on the sheet increased. Therefore, the mechanical

properties of the chitosan nanofiber sheet improved. Of course, the sheet density was also found to affect these mechanical properties. Above 10 cycles, however, the length and crystallinity of the chitosan nanofibers decreased, as mentioned above, resulting in a direct deterioration of the mechanical properties of the sheets.

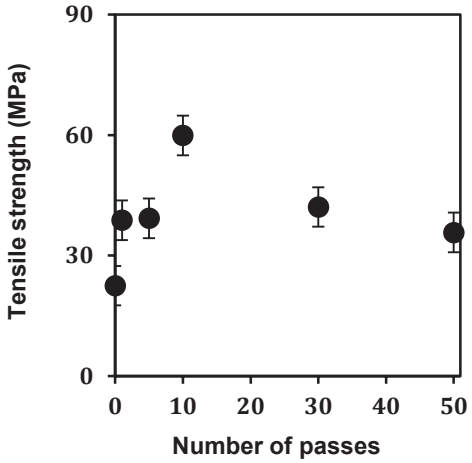


**Figure 32.** Tensile strength of chitosan nanofiber sheets graphed against the number of passes. Reproduced with permission from ref. 90. Copyright 2013, Elsevier.

Figure 33 shows the coefficient of thermal expansion (CTE) values of the chitosan nanofiber sheets. The CTE decreased from 14.0 ppm $K^{-1}$ at 0 passes to 11.2 ppm $K^{-1}$ at 10 passes. In contrast, above 10 passes the CTE increased abruptly, reaching 14.9 ppm $K^{-1}$ at 50 passes. CTE is affected by the morphology and crystallinity of nanofibers. Up to 10 passes, the nanofibers became thinner with additional passes. The fine nanofiber network extending outward in a random manner resulted in a thermal expansion of the nanofibers in all directions, thus reducing the thermal expansion of the sheet. On the other hand, extensive HPWJ treatment reduced the crystallinity of the

nanofibers, which directly increased the thermal expansion.

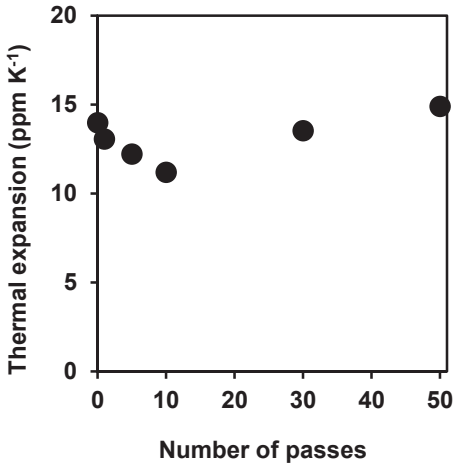


**Figure 33.** Coefficient of thermal expansion of chitosan nanofiber sheets as a function of number of passes. Reproduced with permission from ref. 90. Copyright 2013, Elsevier.

## 4. 4. Conclusion

Herein, the effects of the nano-fibrillation on chitosan by the HPWJ system have been discussed, paying particular attention to the morphology, chemical structure, crystallinity, viscosity, mechanical properties, and thermal expansion of chitosan nanofibers. The chitosan powders turned into thinner nanofibers through the HPWJ system, as the nanofiber aggregate structure was still maintained after deacetylation treatment. Extensive cycles of treatment reduced the fiber length and crystallinity due to the high collision force caused by super high-pressure water. As a result, the mechanical

and thermal expansion properties were improved by nanofibrillation up to 10 passes, while further treatment resulted in a degradation of these properties. These detailed characterizations are expected to play an important role in developing commercial applications for the nanofibers. Naturally rare cationic-charged nanofibers can be obtained from chitosan flakes. The HPWJ system could therefore be a key tool for designing smart materials by means of ionic complex or self-organization approaches. In addition to the chitin and cellulose nanofibers, the chitosan nanofibers have been now listed in bio-nanofibers.

# Chapter 5

## Facile Preparation of Surface *N*-halamine Chitin Nanofiber to Endow Antimicrobial activities

### 5.1 Introduction

Chitin is a natural carbohydrate polymer that abounds in the exoskeletons of crustaceans and in fungal cell walls. Despite chitin's enormous abundance, most crab and prawn shells are thrown away as industrial waste, mainly owing to the insoluble nature of chitin in water. However, Ifuku *et al.* prepared chitin nanofibers (CNFS) by using a mechanical disintegration system and CNFs found to disperse homogeneously in water.[28, 29] The dispersion was easy to handle and to shape into desired forms for specific applications. Taking the advantage of this special property of CNFs they prepared optically transparent CNF composites with acrylic resins.[39] CNF could significantly increase the Young's moduli and the tensile strengths of acrylic resins, and decrease thermal expansion without losing transparency or flexibility by virtue of CNFs' reinforcement effect. Moreover, CNFs have powerful biological activities. For instance, they have anti-inflammatory actions via suppressing NF-κB and MCP-1 activations, and suppress fibrosis in an acute ulcerative colitis mouse model, indicating that CNF is potentially a novel medicine or functional food for patients with inflammatory bowel disease.[81, 82] Furthermore, application of CNF to skin improved the epithelial granular layer and increased granular density and resulted in a lower production of TGF-$\beta$,

indicating that they can be incorporated into the manufacture of cosmetics or textiles.[83] Consequently, we expect that nanochitin with the above-mentioned properties will have increased applicability as a novel bio-material.[25] However, CNFs do not have antimicrobial properties.

*N*-halamine has received much attention owing to its attractive functions, such as its efficacy against microorganisms as well as its stability, rechargeability, and nontoxicity to humans.[84, 85]A covalent bond forms between nitrogen and halogen atoms (N-X) in *N*-halamine-based material. In halamine, chlorine has generally been used to connect with amine, amide, or imide groups due to the ease of modifying chlorine as well as to its safety, its green reaction in water, and its low cost as a reagent.[86-88] Diluted sodium hypochlorite solution, common household bleach, can be used for *N*-chlorination. The antimicrobial properties of *N*-chlorine are the result of the direct transfer of chlorine ions ($Cl^+$) to receptors in the cells of microorganisms. Thus, *N*-halamine can kill microorganisms without the release of free chlorine.[89]

Recently, the author developed a method to isolate CNFs by a simple disintegration system which applied high-pressure water jet technology.[55, 90] The morphological characteristics of CNFs include a thickness of approximately 4 to 6 nm, with efficient mechanical properties owing to its extended crystalline structure and water disperiility.[55, 56] Some researchers have applied *N*-chlorination to chitosan, which is produced by the deacetylation of chitin to obtain antimicrobial chitosan, although chitosan itself has antimicrobial activity in nature.[91, 92] On the other hand, there has been

no report about *N*-halamine-based chitin, although the acetamide group in chitin could be used for *N*-chlorination. This is because chitin is an insoluble powder and difficult to handle as a biomaterial. Since CNFs can homogeneously disperse in water, they can be useful for the reaction. Here, the author demonstrated *N*-halamine CNFs for the first time and used them to endow CNF with antibacterial and antifungal properties (Fig. 34).

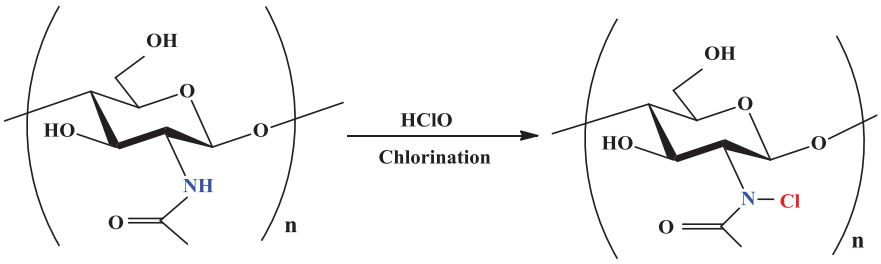


**Figure 34.** Surface *N*-chlorination of chitin nanofiber.

## 5. 2 Experimental

### 5. 2. 1 Materials

*α*-Chitin from crab shell was purchased from Koyo Chemical and used as received. Sodium hypochlorite solution with 5% active chlorine content was from Wako Pure Chemical Industries and was used throughout this study. The other chemicals were analytical grade and used without further purification.

### 5. 2. 2 Preparation of *N*-halamine Chitin Nanofiber Film

CNFs were prepared according to a previously reported method.[55] In brief, dry chitin powder was dispersed in water at 1 wt. %. Acetic acid was added to the chitin dispersion to adjust the pH to 3. It was passed through a high pressure water-jet system (Star Burst Mini, HJP-25001S, Sugino Machine Co., Ltd.), equipped with a ball-collision chamber for mechanical disintegration. The treatment was conducted for 30 cycles for nano-fibrillation. The obtained CNF was dispersed in water at a fiber content of 0.1 wt. %. The water was poured into a glass petri dish and dried at 40 $^{o}$C overnight. The resultant cast film had a uniform surface with a thickness of approximately 25 $\mu$m and a weight of 110 mg. For *N*-chlorination, the CNF film was soaked in a preset amount of sodium hypochlorite solution at room temperature for a predetermined period of time. After *N*-chlorination, the film was washed with deionized water thoroughly and air-dried. The washing water was tested with potassium iodide/starch to ensure that the free chlorine was completely removed.

### 5. 2. 3 Characterization

#### 5. 2. 3. 1. Measurement of Active Chlorine Content

Iodometric titration was employed to determine the active chlorine content loaded onto the CNF film.[93] Approximately 0.05 g of chlorinated CNF was dispersed in 5 mL of deionized water containing 1 wt. % acetic acid. One gram of potassium iodide was added and the mixture was stirred vigorously for 1 h at room temperature. After

then, the titer titrated against the titrant sodium thiosulfate, and 1 mL of 1% starch solution was added as an indicator near the end point. The oxidative chlorine in the film was calculated using the following equation:

$$[Cl^+] = (V \times N \times 35.45)/(W \times 2) \times 100$$

Where $[Cl^+]$ is the wt. % of oxidative chlorine on the CNF, $V$ is the volume of consumed sodium thiosulfate solution in one liter, $N$ is the normality of the titrant (equiv./L), and $W$ is the weight of the chlorinated CNF sample in grams.

### 5. 2. 3. 2 Stability and Rechargeability Test of Chlorinated CNF film

To study the stability of the chlorinated CNF film, the film was stored at 25 $^oC$ and the chlorine content was tested periodically for a 30-day storage time. For the rechargeability test, the film was treated with 0.3% sodium thiosulfate aqueous solution at room temperature for 30 min to quench the active chlorine and then chlorinated again according to the above-mentioned chlorination procedure with sodium hypochlorite.

### 5. 2. 3. 3 Characterization of Chlorinated CNF Film

The infrared spectra of the CNF film and the chlorinated one were recorded with an FT-IR spectrophotometer (Spectrum 65, Perkin-Elmer Japan Co., Ltd.,) equipped with an ATR attachment (diamond/ZnSe crystal) with a resolution of 4 $cm^{-1}$.

X-ray diffraction (XRD) profiles of the samples were obtained with Ni-filtered $CuK_{\alpha}$ from an X-ray generator (Ultima IV, Rigaku) operating at 40 kV and 30 mA. The diffraction profile was detected using an X-ray goniometer scanning from $5^{o}$ to $35^{o}$.

The regular light absorbances of these samples were measured using a UV-Vis spectrophotometer (V550; JASCO, Tokyo, Japan).

The thermal stability of the chlorinated CNF film was studied on a TG/DTA 6300 (Seiko Instruments). The sample weighed approximately 5 mg and was heated in argon at a rate of 10 $^{o}C\ min^{-1}$ up to 500 $^{o}C$.

For field emission scanning electron microscopic (FE-SEM) observation, the CNF film was coated with an approximately 2 nm layer of Pt by an ion sputter coater and observed by FE-SEM (JSM-6700F; JEOL, Ltd.) operating at 2.0 kV.

**5. 2. 3. 4 Antibacterial Activity Test**

*Escherichia coli* (*E. coli,* NBRC 3972, Gram-negative bacteria) and *Staphylococcus aureus* (*S. aureus*, NBRC 12732, Gram-positive bacteria) were used to study the antibacterial properties of the chlorinated CNF films. Both species were purchased from the NITE Biological Resource Centre (Chiba, Japan). We followed the "sandwich" system for antibacterial tests.[85] Polypeptone-yeast broth solution

(polypeptone 1%; yeast extract 0.2%; $MgSO_4$, 0.1%) was used to grow *E. coli* and *S. aureus* for 24 h at 37 $^oC$. The bacteria were harvested by centrifugation, washed twice with phosphate-buffered saline (PBS) (pH 7), and then resuspended in PBS to densities of $10^8$–$10^9$ CFU /mL. The chlorinated CNF films were cut into small pieces (ca. 1 × 1 $cm^2$), and the films were sterilized for 15 min on each side under UV light. Ten microliters of an aqueous suspension containing $10^8$-$10^9$ CFU /mL of *E. coli* or *S. aureus* was placed onto the surface of a film. Another, identical film was used for sandwiching to ensure adequate contact with the bacteria. After a certain period of contact time, the entire sandwich was transferred into 10 mL of 0.03 wt. % sodium thiosulfate aqueous solution. The mixture was vigorously shaken for 5 min and sonicated for 10 min. *Cao et al.* demonstrated that sodium thiosulfate solution at this concentration could quench the active chlorines in the films without affecting the growth of the bacteria.[85] An aliquot of the solution was serially diluted, and 100 $\mu$L of each dilution was plated onto agar plates (Luria Bertani agar for *E. coli*, polypeptone-yeast agar for *S. aureus*). A similar procedure was applied to unchlorinated CNF films as positive controls. Bacterial colonies were counted after incubation at 37 $^oC$ for 24 h.

### 5. 2. 3. 5 Antifungal Activity Test

*Alternaria alternata* (strain O-94) and *Penicillium digitatum* (strain P1), were selected as illustrative examples of fungi for the antifungal activity study of the CNF films following the sandwich system. Both fungi were maintained on potato

dextrose agar (Difco, Detroit, MI, USA) slopes. For antifungal activity tests, spores of *A. alternata* were prepared as previously described.[94] For sporulation, *P. digitatum* was grown on a PDA agar plate at 24°C for 1 week. Upon suspension in PBS, the concentration of fungi was found to be $10^7$ spores /mL. Ten microliters of spore suspension ($10^7$ spores /mL) was placed onto the surface of one of the chlorinated CNF films (1 $cm^2$) and sandwiched by the other. After 24 h of contact time, the entire sandwich was harvested in 5 mL sodium thiosulfate aqueous solution (0.03%) and sorted out as described above. Unchlorinated CNF films were challenged against the same fungal suspension under identical conditions as the positive and negative controls. After incubation for 24 h, the inhibition of spore germination was observed under a light microscope. Each antifungal test was repeated three times.

## 5. 3 Results and Discussion

### 5. 3. 1 Active Chlorine Content of *N*-halamine Chitin Nanofiber

CNF film was treated with diluted sodium hypochlorite solution to introduce chlorine into the acetamide group at the C2 position (Fig. 34). Figure 35 shows the effect of the sodium hypochlorite concentration on the amount of active chlorine content introduced in CNF film with 30 min chlorination time. After NaClO treatment with 0.25% and 0.50% concentrations, the active chlorine content increased steeply to

1.64% and 2.48%, respectively, by the loading of chlorine onto CNF. However, above 0.50% NaClO concentration, the reaction rate decreased, and chlorine content was almost saturated, reaching 2.69% by the 1.00% concentration treatment.

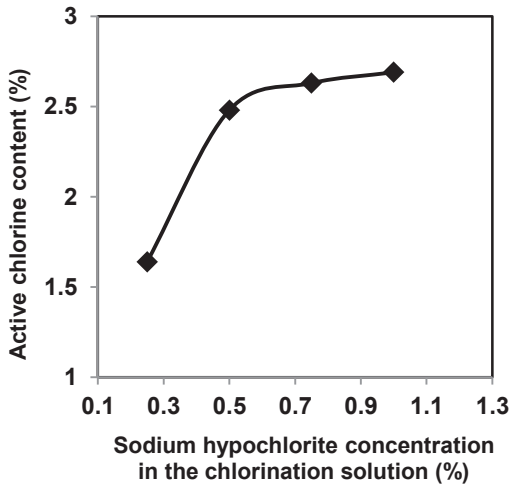


**Figure 35.** Effect of sodium hypochlorite concentration on active chlorine content loaded on chitin nanofiber at 30 min.

Figure 36 shows the effect of chlorination time on the active chlorine content loaded on CNF using 0.50% NaClO diluted solution. The active chlorine content rapidly increased to 1.35% after only 5 min chlorination time, reaching 2.48% after 30 min. However, chlorination times of more than 30 min didn't increase chlorine content effectively.

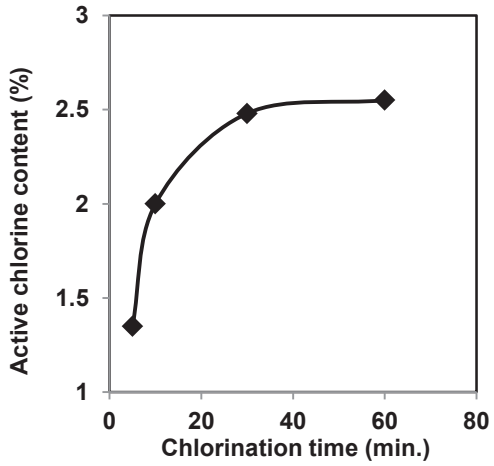


**Figure 36.** Effect of chlorination time on active chlorine content in chitin nanofiber film at 0.5% sodium hypochlorite concentration.

These saturation behaviors in chlorination are caused by the heterogeneous reaction of CNF crystal.[95] First, the CNF surface was preferentially chlorinated with a higher reaction speed, and then the inside crystalline core part of CNF reacted gradually. From Figures 35 and 36, the saturated active chlorine content corresponded to approximately 15% of the degree of substitution (DS). The chlorination DS seems reasonable to a certain extent, since the DS of a surface-modified CNF previously reported was approximately 20%.[96]

### 5. 3 .2 Structural Characterization of *N*-halamine Chitin Nanofiber

The FT-IR spectra of *N*-halamine CNF are shown in Figure 37. After the chlorination reaction of CNF, the amide II band at 1554 $cm^{-1}$ corresponding to the N-H

bending vibration mode was decreased and slightly shifted to 1558 $cm^{-1}$.[97] This is obviously due to the partial substitution of the N-H bond to the N-Cl bond.[98]

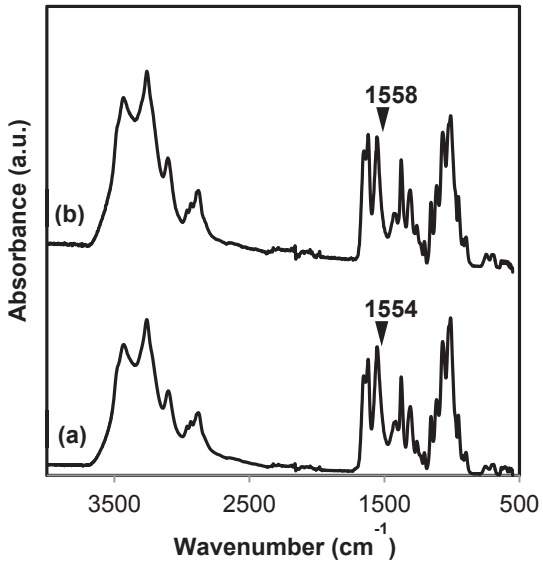


**Figure 37.** FT-IR spectra of (a) chitin nanofiber film and (b) the chlorinated derivative with 2.63% active chlorine content.

The UV-Vis spectra of *N*-halamine CNF film are shown in Figure 38. After chlorination, a broad absorption peak at approximately 320 nm appeared. The peak is known to be caused by the disassociation of the N-Cl bond; the disassociation also provides evidence of *N*-halamine formation of CNF after sodium hypochlorite treatment.[99, 100]

An XRD study was carried out to investigate the effect of the chlorination treatment on the crystalline structure of CNF. Figure 39 shows the diffraction profile of

*N*-halamine-based CNF film. After chlorination, all diffraction peaks observed at 9.2°, 19.2°, 20.7°, and 22.8° coincided with those of the original CNF. They were typical antiparallel crystal patterns of $\alpha$-chitin.[37] Therefore, the chlorination did not change the crystalline structure of CNF, thus indicating that chlorination took place on the surface of CNF, as mentioned above.

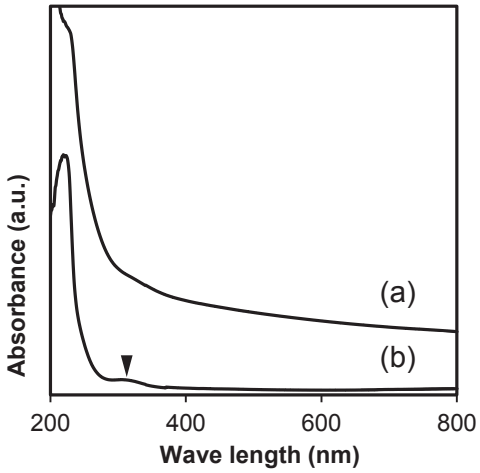


**Figure 38.** UV-Vis spectra of (a) chitin nanofiber film and (b) the chlorinated derivative with 2.63% active chlorine.

Figure 40 displays derivative TGA curves of CNF films before and after sodium hypochlorite treatment. The original CNF film showed a single degradation peak at 348 °C. On the other hand, the chlorinated sample had a major broad degradation peak in the range of around 300-360 °C and a minor degradation peak at 155 °C. The major degradation would correspond to the decomposition of unchlorinated CNF. The minor degradation at 155 °C would be due to the decomposition of the *N*-halamine part on the CNF surface, since the association energy of the N-Cl bond is

lower than that of the N-H bond.[101, 102] Thus, chlorination accelerated the thermal decomposition of chitin.

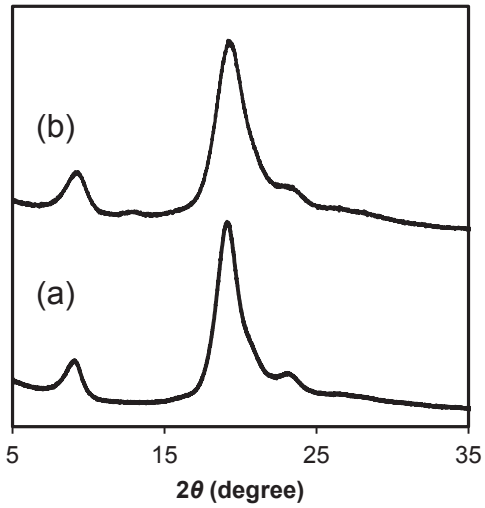


**Figure 39.** X-ray diffraction profiles of (a) chitin nanofiber film and (b) the chlorinated derivative with 2.63% active chlorine content.

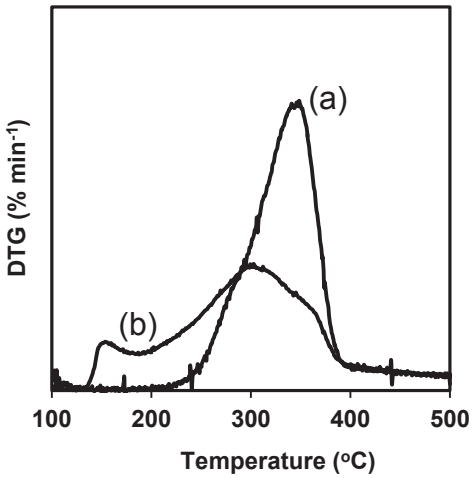


**Figure 40.** Derivative TG analysis of (a) chitin nanofiber film and (b) the chlorinated derivative with 2.63% active chlorine content.

FE-SEM images of the CNF before and after chlorination are shown in Figure 41. The characteristic nanofiber morphology was maintained after the reaction. The fiber width was also similar to that of the original CNF. Similar fiber width also indicates that balky chlorine was introduced on the CNF surface.

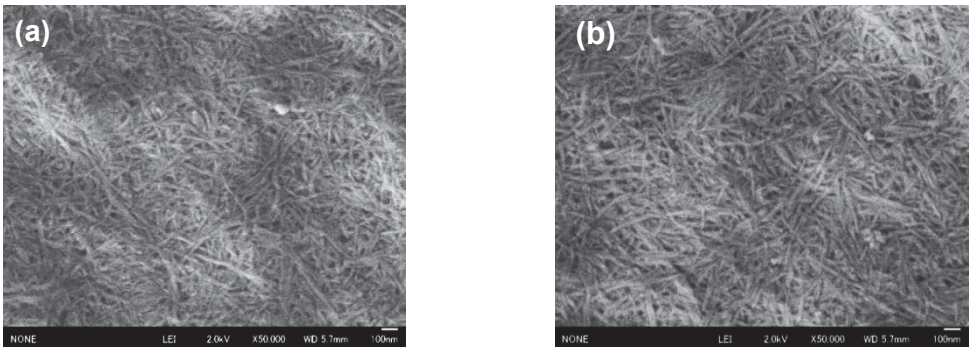


**Figure 41.** SEM images of (a) chitin nanofiber film and (b) the chlorinated derivative with 2.63% active chlorine content.

The stability and rechargeability of the *N*-halamine CNF film was studied (Fig. 42). The active chlorine content of freshly prepared *N*-halamine CNF film was 2.69%. The content gradually decreased with increasing storage time due to the disassociation of the N-Cl bond and became 2.0% after 15 days of storage. However, further storage up to 30 days total did not remarkably reduce the chlorine content. After 30 days of storage, we could introduce chlorine on the CNF surface again by another sodium hypochlorite treatment. After the second chlorination treatment under the same conditions, the active chlorine content was recovered to 2.60%. Thus, chlorinated CNF has excellent rechargeability to recover antimicrobial and antifungal activity to be as described next.

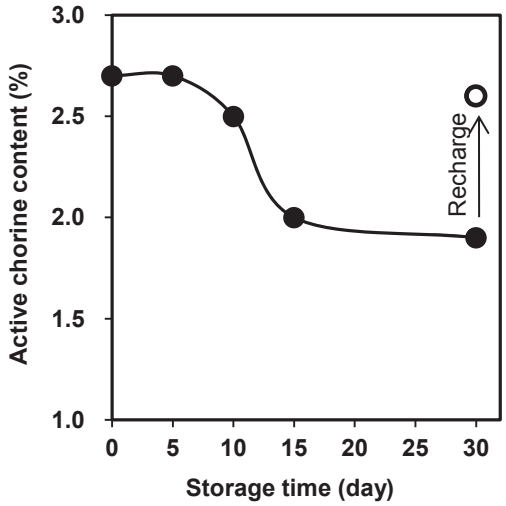


**Figure 42.** Storage stability and recharge-ability of chlorinated chitin nanofiber film.

### 5. 3. 3 Antimicrobial and Antifungal Efficacy

Table 9 presents the biocidal efficacy results of unchlorinated and chlorinated CNF films against Gram-negative *E. coli* and Gram-positive *S. aureus*. CNF films containing 2.69% of active chlorine were challenged with $10^8$-$10^9$ CFU /mL each of *S. aureus* and *E. coli*, respectively. Data showed that the efficacy of the films increased as the contact time increased, and about a 100% kill rate for *E. coli* was achieved within just 10 min of contact time. However, all the microbes of the stated bacterial species died within 30 min, which was treated as a total kill, within the contact area of the chlorinated films. On the other hand, the unchlorinated CNF film did not show any antimicrobial activity against these pathogens, even after 60 min of contact time. This reminds us that chitin nanofibers have no antibacterial functions.

**Table 9.** Percentage reduction of *E. coli* and *S. aureus*.

| Contact Time (min) | *E. coli* [a] (%) | | *S. aureus* [a] (%) | |
|---|---|---|---|---|
| | Unchlorinated CNF film | Chlorinated CNF film[b] | Unchlorinated CNF film | Chlorinated CNF film[b] |
| 5 | 0 | 86.4 | 0 | 46.7 |
| 10 | 0 | 99.9 | 0 | 87.8 |
| 30 | 0 | Total killed | 0 | Total killed |
| 60 | 0 [c] | Total killed | 0 [c] | Total killed |

[a] *E. coli* and *S. aureus* concentration were $10^8$-$10^9$ CFU /mL.

[b] The chlorinated CNF film contained 2.69 % of active chlorine.

[c] Compared with the antibacterial result of cellulose membrane, which was used as the negative control in the antimicrobial study.

*A. alternata* is a mainly saprophytic fungus, but it is also known as a plant pathogen and as an allergen in humans. On the other hand, *P. digitatum* is a common postharvest pathogen causing a green mold on citrus fruits. The antifungal activity of chlorinated CNF films was assessed by the percentage inhibition of spore germination (Fig. 43) of an individual fungus, where the original spore concentration was $10^7$ spores /mL. The most striking finding was that the chlorinated CNF film inhibited the growth of *A. alternata* spores by almost 100% compared with the controls. In contrast, the germination of *P. digitatum* spores was more difficult to stop, 80% of the spores were

inhibited. We stated earlier that spores were sandwiched between CNF films for 24 h and that the accuracy of the results was verified by Tukey's Test ($P < 0.05$). These findings are fascinating, as the transfer of oxidative chlorine from the CNF films to the appropriate receptors in microorganisms could effectively destroy or inhibit the enzymatic or metabolic process, leading to the expiration of the microorganisms.

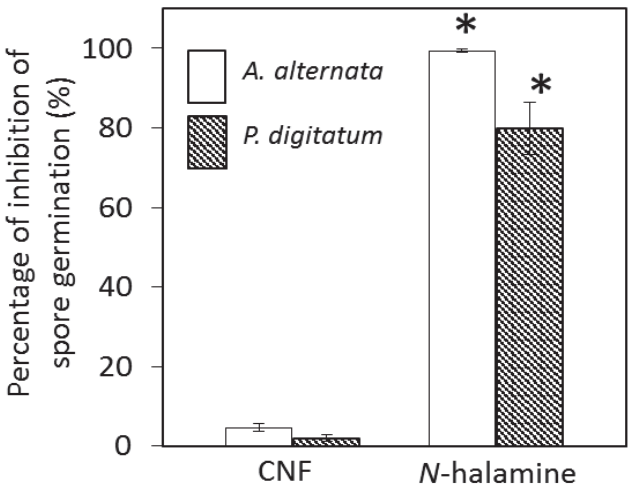


**Figure 43.** Antifungal effect of chlorinated CNF films with 2.69% active chlorine content. Spores were sandwiched between CNF film for 24 h. Spores were harvested and placed on cellulose membrane for microscopic observation. Data represent the mean of three independent experiments and error bars. Asterisks indicate significant differences with Tukey's test between films ($P<0.05$).

## 5. 4 Conclusion

*N*-halamine-based CNF film was prepared successfully by using easily available diluted sodium hypochlorite. The concentration of sodium hypochlorite and the reaction time strongly affected the active chlorine content on the films. FT-IR, UV-Vis, XRD, and TGA analyses showed the presence of a N-Cl bond on the CNF surface. Chlorine was rechargeable onto CNF by the same sodium hypochlorite treatment. All the microbes of *E. coli* and *S. aureus* died within 30 min of contact with the chlorinated CNF film. Moreover, 100% of *A. alternata* and 80% of *P. digitatum* fungal spore stopped their germination upon 24 h treatment with the chlorine-containing CNF films. Here, CNF acquired antibacterial and antifungal properties in addition to various characteristics, such as nanostructure, high surface area, excellent mechanical properties, and several biological properties. Chlorination is expected to expand the range of commercial applications of CNF, especially in medical, food, and cosmetics fields.

# General Summary

The two most abundant natural polymers on earth, cellulose and chitin have attracted increasing attention as a source of renewable energy and functional materials and together represent the most abundant materials in nature. In addition, nanofibers are considered as one of the leading ingredients for designing materials of 21 st century. Therefore, research and developments on nanofibers has gained significant importance, in recent years. Currently, the most commonly used process for manufacturing nanofibers is the electrospinning process, known as bottom-up approach. Nonetheless, bionanofibers isolated by the top-down process have remarkable advantages in terms of their high crystallinity, reproducibility, biodegradability, and biocompatibility.

This study deliberately searched for environmental caring materials, as well as an eco-friendly, facile synthetic pathway for the production of nanofibers.

Chapter 1 contained the preparation of $\alpha$-chitin nanofibers by suing several passes of HPWJ system to investigate the effects of passes on nanofibrillation. SEM observation, as well as the light transmittance of chitin nanofibers slurry and the nanocomposite with acrylic resin, indicated that the nanofibers became thinner as the number of passes increased. SEM observations also revealed that even at 5 passes major amount of nano-fibrillation took place, which remarkably ended at around 10 passes. Individualized nanofibers with a cross-sectional width of 5-6 nm were distinguished, depending on the number of passes. Surprisingly, nanofibers with $\leqq$ 1 nm widths were

observed in many occasions. However, above 30 passes, the fibers thickness did not change meaningfully. Besides, SEM images and the viscosity of the nanofibers presented that the fibers length decreased because the fibers began to break above 30 passes. The results of molecular weight determination exhibited that until 30 passes molecular weight decreased gradually and these variations matched well with the morphological changes of chitin nanofibers. The mechanical properties of chitin nanofibers sheets were improved by increasing the number of passes up to 30, but further treatment did not improve these properties. However, XRD measurement indicated that the HPWJ System did not damage the crystalline part of the chitin fibers.

Chapter 2 stated the simple preparation of *β*-chitin nanofiber from squid pen powder where HPWJ technology employed for nano-fibrillation. SPM observations revealed that disintegration remarkably ended at around 10 passes, and the nanofibers became thinner to some extent. The above observations were also supported by the transmittance and viscosity records of chitin nanofibers slurry. Individualized nanofibers with 3-4 nm cross-sectional width were distinguished, based on the number of passes. XRD measurements indicated that both the crystalline structure and crystallinity of chitin nanofibers retained after the HPWJ treatments. Young's moduli of *β*-chitin nanofiber sheets were improved with increasing the number of passes, although, the tensile strength increased up to 10 passes, and further cycles of treatments result a direct loss of this property.

In chapter 3, chitin nanocrystals were isolated by hydrolysis with sulfuric acid (S-CNC) and phosphoric acid (P-CNC) successively from chitin powder. Isolated nanocrystals were characterized and compared with the naocrystals prepared by the conventional HCl hydrolysis (H-CNC). SPM images revealed that homogeneous formation of nanocrystals and their shapes strongly depends on chitin to acid ratio, as well as hydrolysis time. Mostly individualized CNCs have a cross-sectional width of 9.3 nm (H-CNC), 8 nm (S-CNC) and 7.3 nm (P-CNC). Besides, P and S-CNCs crystallinity (93.4 and 92.6%) are remarkably higher than that of H-CNCs (70%). Nonetheless, all types of CNCs formed stable dispersion in water and had a high transparency. Thermogravimetric analysis illustrated that P-CNC have higher thermal stability with a sharp decomposition at 378.5 $^{o}$C, compared with the native H and S-CNC. Elemental analysis data and the char formation of S-CNC at 500 $^{o}$C, symbolizes in favor of small amount of surface functionalization.

Chapter 4 demonstrated facile preparation of chitosan nanofibers from chitosan powder using a “top-down” approach. The morphological changes of nanofibers were examined by the SEM observations and found that the chitosan nanofibers nanofibrillation improved gradually as the number of passes increased by the HPWJ system. However the fiber thickness did not change significantly above 10 passes. Crystallinity and the chitosan nanofiber length decreased after extensive treatment generally at around 30 passes due to the strong collision forces generated by the system. The mechanical properties and thermal expansion of the chitosan nanofiber sheets were improved by increasing the number of passes up to 10, even though further treatment results a significant loss of these properties.

Chapter 5 contained unique character as the surface of chitin nanofibers (CNF) converted to *N*-halamine for the first time to judge the antimicrobial efficacy. Modification was achieved by soaking the CNF film in sodium hypochlorite solution at room temperature. FT-IR, UV-Vis, and TG analysis showed the presence of N-Cl bond on the surface of CNF. However, the nanofibers morphology did not damage after the chlorination treatment. *N*-halalmine based CNF film showed strong efficacy against both the gram- negative (*E. coli*) and gram- positive (*S. aureus*) and within 30 min of contact time, the total kill of the microbes were noted. CNF film with N-Cl bond also proved strong inhibition growth of *A. alternata* (100%) and *P.digitatum* (80%). The obtained fascinating results hopefully will expand the application of CNF as biomaterials.

# References


(1) K. G. Nair, and A. Dufresne, Crab shell chitin whisker reinforced natural rubber nanocomposites. 1. Processing and swelling behavior. *Biomacromolecules* 4, 657-665 (**2003**).

(2) M. Rinaudo, Chitin and chitosan: Properties and applications. *Prog. Polym. Sci.* 31, 603–632, **(2006).**

(3) V. K. Mourya, and N. N. Inamdar, Chitosan-modifications and applications: opportunity galore. *React. Funct. Polym.* 68, 1013-1051 (**2008**).

(4) R. Jayakumar, D. Menon, K. Manzoor, S. V. Nair, and H. Tamura, Biomedical applications of chitin and chitosan based nanomaterials- A short review. *Carbohydrate Polymers* 82, 227-232 **(2010)**.

(5) F. Shahidi, J .K. V. Archchi, and Y. J. Jeon, Food applications of chitin and chitosan. *Tren. Food Sci. Technol.*10, 37-51 (**1999**).

(6) M. Mincea, A. Negrulescu and V. Ostafe, Preparation, modification, and applications of chitin nanowhiskers: a review. *Red. Adv. Mater. Sci.* 30, 225-242 (**2012**).

(7) J. B. Jeng, Y. S. He, S. L. Li, and Y. Z. Wang, Chitin whiskers: An overview. *Biomacromolecules* 13, 1-11 (**2012**).

(8) W. Suginta, P. Khunkaewla, and A. Schulte, Electrochemical biosensor applications of polysaccharides chitin and chitosan. *Chem. Rev.* 113, 5458−5479 (**2013**).

(9) K. M. Rudall and M. W. Kenchington, The chitin system. *Biol. Rev.* 48, 597-633 **(1973)**.

(10) K. M. Rudall, The chitin/protein complexes of insect cuticles. *Adv. Insect. Physiol.*1, 257-313 (**1963**).

(11) Y. Ogawaa, S. Kimura, and M. Wada, Electron diffraction and high-resolution imaging on highly-crystalline *β*-chitin microfibril. *J. Struc. Biol.*176, 83-90 (**2011**).

(12) P. Jolles, and R. A. A. Muzzarelli, Chitin and Chitinases. Birkhauser: Basel, Switzerland, p1(**1999**).

(13) S. S. Ojha, D. R. Stevens, T. J. Hoffman, K. Stano *et al.,* Fabrication and characterization of electrospun chitosan nanofibers formed via templating with polyethylene oxide. *Biomacromolecules* 9*,* 2523–2529 (**2008**).

(14) R. Jayakumar, N. Nwe, S. Tokura, and H. Tamura, Sulfated chitin and chitosan as novel biomaterilas. *Int. J. Biol. Macromol.* 40, 175-181 **(2007)**.

(15) S. Mallick, S. Sharma, M. Banerjee, S. S. Ghosh, A. Chattopadhyay, and A. Paul, Iodine-stabilized Cu nanoparticle chitosan composite for antibacterial applications. *ACS Appl. Mater. Interfaces* 4, 1313−1323 (**2012**).

(16) H. K. No, S. P. Meyers, W. Prinyawiwatkul, and Z. Xu, applications of chitosan for improvement of quality and shelf life of foods: a review. *J Food Sci.* 72, R87-99 **(2007).**

(17) P. K. Dutta, S. Tripathi , G. K. Mehrotra , J. Dutta, Perspectives for chitosan based antimicrobial films in food applications. *Food Chemistry* 114, 1173–1182 (**2009**).

(18) S. H. Lim, and S. M. Hudson, Review of chitosan and its derivatives as antimicrobial agents and their uses as textile chemicals. *J. Macromol. Sci. PC.* 43, 223-269 **(2003).**

(19) A. Bhatnagar , and M. Sillanpää, Applications of chitin- and chitosan- derivatives for the detoxification of water and wastewater—A short review. *Adva. Coll. Inter. Sci.* 152, 26-38 **(2009).**

(20) M. Alaibadi, M. Irani, J. Ismaeili, H. Piri, and M.J. Parnian, Electrospun nanofiber membrane of PEO/Chitosan for the adsorption of nickel, cadmium, lead and copper ions from aqueous solution. *Chem. Eng. J.* 220, 237-243 (**2013**).

(21) P. M. Visakh, and S. Thomas, Preparation of bionanomaterials and their polymer nanocomposites from waste and biomass. *Waste Biomass Valor* 1, 121-134 (**2010**).

(22) R. Jayakumar, M. Prabhahan, S. V. Nair, and H. Tamura, Novel chitin and chitosan nanofibers in biomedical applications. *Biotechnol. Adv.* 28, 142 -150 (**2010**).

(23) T. J. Sill, and H. A. Recum, Electrospinning: Applications in drug delivery and tissue engineering. *Biomaterials* 29, 1989-2006 (**2008**).

(24) K. Desai, K. Kit, J. Li, P. M. Davison, S. Zivanovich, and H. Meyer, Nanofibrous chitosan non-oven for filter applications. *Polymer* 50, 3661-3669 (**2009**).

(25) S. Ifuku, and H. Saimoto, Chitin nanofibers: Preparations, modifications, and applications. *Nanoscale* 4, 3308-3318 (**2012**).

(26) B. M. Min, S. W. Lee, J. N. Lim, Y. You, T. S. Lee, P. H. Kang, and W. H. Park, Chitin and chitosan nanofibers: Electrospinning of chitin and deacetylation of chitin nanofibers. *Polymer* 45, 7137- 7142, **(2004).**

(27) H. Zhao, X. Feng, and H. Gao, Ultrasonic technique for extracting nanofibers from natural materials. *Appl. Phys. Let.* 90, 073112, **(2007).**

(28) S. Ifuku, M. Nogi, K. Abe, M. Yoshioka, M. Morimoto, H. Saimoto and H. Yano, Preparation of chitin nanofibers with a uniform width as $\alpha$-chitin from crab shells. *Biomacromolecules* 10, 584-1588 **(2009).**

(29) S. Ifuku, M. Nogi, K. Abe, M. Yoshioka, M. Morimoto, H. Saimoto and H. Yano, Simple preparation method of chitin nanofibers with a uniform width of 10 to 20 nm from prawn shell under the neutral conditions. *Carbohydrate Polymers* 84, 762-764 **(2011).**

(30) S. Ifuku, R. Nomura, M. Morimoto and H. Saimoto, Preparation of chitin nanofibers from mushrooms. *Materials* 4, 1417-1425 **(2011).**

(31) S. Ifuku, M. Nogi, M. Yoshioka, M. Morimoto, H. Yano, and H. Saimoto, Fibrillation of dried chitin into 10-20 nm nanofibers by a simple method under acidic conditions. *Carbohydrate Polymers* 81, 134-139 (**2010**).

(32) Y. Watanabe, S. Kitamura, K. Kawasaki, T. Kato, K. Uegaki, K. Ogura, and K. Ishikawa, Application of a water jet system to the pretreatment of cellulose. *Biopolymers* 95, 833-839 (**2011**).

(33) R. Kose and T. Kondo, Favorable 3D-network formation of chitin nanofibers dispersed in water prepared using aqueous counter collision. *Sen-I Gakkaishi* 67, 91 (**2011**).

(34) S. Ifuku, K. Yamada, M. Morimoto, and H. Saimoto, Nanofibrillation of dry chitin powder by Star Burst system. *J. Nanomater.* 2012, 1-7 (**2012**).

(35) Y. Zhang, C. Xue, Y. Xue, R. Gao and X. Zhang, Determination of the degree of deacetylation of chitin and chitosan by X-ray powder diffraction. *Carbohydrate Research* 340, 1914–1917 **(2005).**

(36) M. Poirier and G. Charlet, Chitin fraction and characterization in N, N-dimethylacetamide/lithium chloride solvent system. *Carbohydrate Polymers* 50, 363-370, **(2002).**

(37) R. Minke and J. Blackwell, The structure of $\alpha$-Chitin. *J. Mol. Biol.* 120, 167-181 **(1978**).

(38) J. Vincent and U. Wegst, Design and mechanical properties of insect cuticle. *Arthro. Struc. Devel.* 33, 187-199 (**2004**).

(39) M. Wada and Y. Saito, Lateral thermal expansion of chitin crystals. *J. Appl. Polym. Sci. Part B: Polym. Phys.* 39, 168-174 (**2001**).

(40) H. Yano, J. Sugiyama, A. N. Nakagaito, M. Nogi, T. Matsuura, M. Hikita and K. Handa, Optically transparent composites reinforced with networks of bacterial nanofibers. *Adv. Mater.* 17, 153-155 (**2005**).

(41) S. Ifuku, S. Morooka, A. N. Nakagaito, M. Morimoto, and H. Saimoto, Preparation and characterization of optically transparent chitin nanofiber/(meth)acrylic resin composites. *Green Chemistry* 13, 1708-1711 (**2011**).

(42) M. I. Shams, S. Ifuku, M. Nogi, T. Oku, and H. Yano, Fabrication of optically transparent chitin nanocomposites. *Applied Physics A* 102, 325-331 (**2011**).

(43) J. Blackwell, K. H. Gardner, F. J. Kolpak, R. Minke, W. B. Claffey, Refinement of cellulose and chitin structure. *ACS Symp. Ser*. 141, 315-334 (**1980)**.

(44) N. Nishiyam, Y. Noishiki, and M. Wada, X-ray structure of anhydrous *β*-chitin at 1A˚ resolution. *Macromolecules* 44, 950-957(**2011**).

(45) Z. M. Huang, Y. Z. Zhang, M. Kotaki, and S. Ramakrishna **,** A review on polymer nanofibers by electrospinning and their applications in nanocomposites. *Comps. Sci. Technol.* 63, 2223-2253 (**2003**).

(46) S. Ramakrishn, K. Fujihara, W. E. Teo, T. Yong, Z. Ma, and R. Ramaseshan, Electrospun nanofibers : solving global issue. *Mater. Today* 9, 40-50 **(2006).**

(47) D. R. Paul, and L. M. Robeson, Polymer nanotechnology: Nanocomposites. *Polymer* 49, 3187-3204 **(2008).**

(48) A. Sÿturcova´, G. R. Davies, and S. J. Eichhorn, Elastic modulus and stress-transfer properties of tunicate cellulose whiskers. *Biomacromolecules* 6, 1055-1061**(2005)**.

(49) R. Rusli and S. J. Eichhorn, Determination of the stiffness of cellulose nanowhiskers and the fiber-matrix interface in a nanocomposite using Raman spectroscopy. *Appl. Phys Lett.* 93, 033111 **(2008).**

(50) V. Beachleya, and X. Wen, Polymer nanofibrous structures: Fabrication, biofunctionalization, and cell interactions. *Progr. Polym. Sci.* 35, 868-892 **(2010)**.

(51) K. Kurita, K. Tomita, T. Tada, S. Ishii, S. Nishimura, and K. Shimoda , Squid chitin as a potential alternative chitin source: Deacetylation behavior and characteristic properties. *J. Polym. Sci. Part A: Polym. Chem*. 31, 485-491 **(1993)**.

(52) K. Kurita, K. Tomita, T. Tada, S. Ishii, S. Nishimura, and K. Shimoda , *β*-chitin as a convenient starting material for acetolysis for efficient preparation of *N*-acetylchitooligosaccharides. *J. Polym. Sci. Part A: Polym. Chem*. 31, 2393-2395 **(1993)**.

(53) K. Kurita, K. Tomita,T. Tada, S. Ishii, S. Nishimura, and K. Shimoda, Reactivity characteristics of squid *β*-chitin as compared with those of shrimp chitin: High potentials of squid chitin as a starting material for facile chemical modifications. *J. Polym. Sci. Part A: Polym. Chem*. 32, 1027-1032 **(1994)**.

(54) Y. Fan, T. Saito, and A. Isogai, Preparation of chitin nanofibers from squid pen *β*-chitin by simple mechanical treatment under acid conditions. *Biomacromolecules* 9, 1919-1923 **(2008).**

(55) A. K. Dutta, K. Yamada, H. Izawa, M. Morimoto, H. Saimoto, and S. Ifuku, Preparation of chitin nanofibers from dry chitin powder by Star Burst system:

Dependence on number of passes. *J. Chitin Chitosan Sci.* 1, 59-64 **(2013)**.

(56) A. K. Dutta, H. Izawa, M. Morimoto, H. Saimoto, and S. Ifuku, Fibers Width and Molecular Weight Studies of *α*-Chitin Nanofibers. *J. Chitin Chitosan Sci.* 1, 192-196 (**2013**).

(57) S. C. Tjong and Y. Z. Meng, Mechanical and thermal properties of polycarbonate composites reinforced with potassium titanate whiskers. *J. Appl. Polym. Sci.* 72, 501-508 (**1999**).

(58) J. -F. Revol, and R. H. Marchessault, In vitro chiral nematic ordering of chitin crystallites**.** *Int. Jour. Biol. Macromol.* 15, 329-335, **(1993).**

(59) M. Paillet and A. Dufresne, Chitin whisker reinforced thermoplastic nanocomposite. *Macromolecules* 34, 6527-6530 (**2001**).

(60) A. Morin and A. Dufresne, Nanocomposites of chitin whiskers from *Riftia* tubes and poly(caprolactone). *Macromolecules*, 35, 2190-2199 (**2002**).

(61) Y. S. Lu, L. H. Weng, and L. N. Zhang, Morphology and properties of soy protein isolate thermoplastic reinforce with chitin whisker. *Biomacromolecules* 5, 1046-1051 (**2004**).

(62) K. G. Nair, and A. Dufresne, Crab shell chitin whisker reinforced natural rubber nanocomposites. 2. Mechanical behavior. *Biomacromolecules* 4, 666-674 (**2003**).

(63) L. Feng, Z. Zhou, A. Dufresne, J. Huang, M. Wei, and L. An, Structure and properties of new thermoforming bionanocomposites based on chitin whisker-graft-polycaprolactone. *J. Appl. Polym. Sci.* 112, 2830-2837 (**2009**).

(64) P. Hariraksapitak and P. Supaphol, Preparation and properties of α-chitin-whisker-reinforced hyaluronan–gelatin nanocomposite scaffolds. *J. Appl. Polym. Sci.* 117, 3406-3418 (**2010**).

(65) P. R. Chang, R. Jian, J. Yu, and X. Ma, Starch-based composites reinforced with novel chitin nanoparticles. *Carbohydr. Polym.* 80, 420-425 (**2010**).

(66) J. Sriupayo, P. Supaphol, J. Blackwell, and R. Rujiravanit, Preparation and characterization of α-chitin whisker-reinforced chitosan nanocomposite films with or without heat treatment. *Carbohydrate Polymers* 62, 130-136 (**2005**).

(67) J. Sriupayo, P. Supaphol, J. Blackwell, and R. Rujiravanit, Preparation and characterization of α-chitin whisker-reinforced poly(vinyl alcohol) nanocomposite films with or without heat treatment. *Polymer* 46, 5637-5644 (**2005**).

(68) J. D. Goodrich and W. T. Winter, α-Chitin nanocrystals prepared from shrimp shells and their specific surface area measurement. *Biomacromolecules* 8, 252-257 (**2007**).

(69) A. Watthanaphanit, P. Supaphol, H. Tamura, S. Tokura, and R. Rujiravanit, Fabrication, structure, and properties of chitin whisker-reinforced alginate nanocomposite fibers. *J. Appl. Polym. Sci.*110, 890-899 (**2008**).

(70) A. Watthanaphanit, P. Supaphol, H. Tamura, S. Tokura, and R. Rujiravanit, Wet-spun alginate/chitosan whiskers nanocomposite fibers: Preparation, characterization and release characteristic of the whiskers. *Carbohydrate Polymers* 79, 738-746 (**2010**).

(71) J. Junkasem, R. Rujiravanit, B. P. Grady, and P. Supaphola, X-ray diffraction and dynamic mechanical analyses of $\alpha$-chitin whisker-reinforced poly (vinyl alcohol) nanocomposite nanofibers. *Polym. Int.* 59, 85-91 (**2010**).

(72) S. Phongying, S. Aiba, and S. Chirachanchai, Direct chitosan nanoscaffold formation via chitin whiskers. *Polymer* 48, 393-400 (**2007**).

(73) R. A. A. Muzzarelli, P. Morganti, G. Morganti, P. Palombo, M. Palombo, G. Biagini, et al., Chitin nanofibrils/chitosan glycolate composites as wound medicaments. *Carbohydrate Polymers* 70, 274-284 (**2007**).

(74) S. C. Espinosa, T. Kuhnt, E. J. Foster, and C. Weder, Isolation of thermally stable cellulose nanocrystals by phosphoric acid hydrolysis. *Biomacromolecules* 14, 1223-1230 (**2013**).

(75) A. K. Dutta, H. Izawa, M. Morimoto, H. Saimoto, and S. Ifuku, Simple preparation of chitin nanofibers from dry squid pen $\beta$-chitin powder by star burst system. *J. Chitin Chitosan Sci.* 1, 186-191 (**2013**).

(76) Z. M. Huang, Y. Z. Zhang, M. Kotaki, and S. Ramakrishn, A review on polymer nanofibers by electrospinning and their applications in nanocomposites. *Comp. Sci. Technol.* 63, 2223-2253 (**2003**).

(77) K. Y. Lee, L. Jeong, Y. O. Kang, S. O. Lee, and W. H. Park, Electrospinning of polysachharides for regenerative medicine. *Adv. Drug Del. Rev.* 61, 1020-1032 (**2009**).

(78) B. Duan, C. Dong, K. Yao *et al*., Electrospinning of chitosan solutions in acetic acid with poly(ethylene oxide). *J. Biomat. Sci. Polym. Edi.* 15, 797-811 (**2004**).

(79) T. Lin, J. Fang, H. Wang, T. Cheng, and X. Wang, Using chitosan as a thickener for electrospinning dilute PVA solutions to improve fiber uniformity. *Nanotechnology* 17, 3718-3723 (**2006**).

(80) A. K. Dutta, H. Izawa, M. Morimoto, H. Saimoto, and S. Ifuku, Novel preparation of chitin nanocrystals by $H_2SO_4$ and $H_3PO_4$ hydrolysis followed by high-pressure water jet treatments. *J. Chitin Chitosan Sci.* (**in Press**).

(81) K. Azuma, T. Osaki, T. Wakuda, S. Ifuku, H. Saimoto, T. Tsuka, T. Imagawa, Y. Okamoto, and S. Minami, Beneficial and Preventive Effect of Chitin nanofibrils in a dextran sulfate sodium-induced acute ulcerative colitis model. *Carbohydrate Polymers* 87, 1399-1403 (**2012**).

(82) K. Azuma, T. Osaki, S. Ifuku, H. Saimoto, T. Tsuka, T. Imagawa, Y. Okamoto, and S. Minami, $\alpha$-Chitin nanofibrils improve inflammatory and fibrosis responses in inflammatory bowel disease mice model. *Carbohydrate Polym*ers 90, 197-200 (**2012**).

(83) I. Ito, Osaki, S. Ifuku, H. Saimoto, Y. Takamori, S. Kurozumi, T. Imagawa, K. Azuma, T. Tsuka, Y. Okamoto, and S. Minami, Evaluation of the Effects of Chitin nanofibrils on skin function using skin models. *Carbohydrate Polymers* 101, 464-470 (**2014**).

(84) S. D. Worley, F. Li, R. Wu, J. Kim, C. I. Wei, J. F. Williams, J. R. Owens, J. D. Wander, A. M. Bargmeyer, and M. E. Shirtliff, A novel *N*-halamine monomer for preparing biocidal polyurethane coatings. *Surf. Coat. Int. Part B: Coat. Trans.* 86, 273-277 **(2003)**.

(85) H. B. Kocer, S. D. Worley, R. M. Broughton, and T. S. Huang, A novel *N*-halamine acrylamide monomer and its copolymers for antimicrobial coatings. *Reac. Func. Polym.* 71, 561-568 **(2011)**.

(86) S. D. Worley, and D. E.Williams, Halamine water disinfactants. *Cric. Rev. Environ.Control* 18,133-175 **(1998)**.

(87) S. D. Lauten, H. Sarvis, W. B. Wheatley, D. E. Williams, E. C. Mora, and S. D. Worley, Efficacies of Novel *N*-Halamine disinfectants against salmonella and pseudomonas species. *Appl. Environ. Microb*. 58, 1240-1243 (**1992**).

(88) Z. Cao, and Y. Sun, Polymeric *N*-Halamine Latex Emulsions for use in antimicrobial paints. *ACS Appl. Mater. Interfaces* 1, 494-504 (**2009**).

(89) K. Barnes, J. Liang, R. Wu, S. D. Worley, J. Lee, R. M. Broughton, and T. S. Huang, Synthesis and antimicrobial applications of 5,5′-ethylenebis[5-methyl-3-(triethoxysilylpropyl)hydantoin]. *Biomaterials* 27, 4825-4830 (**2006**).

(90) A. K. Dutta, N. Kawamoto, G. Sugino, H. Izawa, M. Morimoto, H. Saimoto, and S. Ifuku, Simple preparation of chitosan nanofibers from dry chitosan powder by the Star Burst system. *Carbohydrate Polymers* 97, 363-367 (2013).

(91) R. Li, P. Hu, X. Ren, S. D. Worley, and T. S. Huang, Antimicrobial N-halamine modified chitosan films. *Carbohydrate Polymers* 92, 534-539 **(2012)**.

(92) Z. Cao, and Y. Sun, N-halamine-based chitosan: Preparation, characterization, and antimicrobial function. *J. Biomed. Mater. Res. Part A* 85, 99-107 **(2008)**.

(93) R. D Johnson, L. Johnson, Y. Itoh, M. Kodama, H. Otani, and K. Kohmoto, Cloning and characterization of a cyclic peptide synthetase gene from *Alternaria alternata* apple pathotype whose product is involved in AM-Toxin synthesis and pathogenicity. *Mol. Plant. Microbe In.* 13, 742-753 (**2000**).

(94) N. K. Gopalan, and A. Dufresne, Nanocomposites of chitin whiskers from *Riftia* tubes and poly(caprolactone). *Biomacromolmolecules* 4, 657-665 (**2003**).

(95) S. Ifuku, S. Morooka, M. Morimoto, and H. Saimoto, Acetylation of chitin nanofibers and their transparent nanocomposite films. *Biomacromolecules* 11, 1326-1330 (**2010**).

(96) S. Ifuku, N. Suzuki, H. Izawa, M. Morimoto, and H. Saimoto, Surface phthaloylation of chitin nanofiber in aqueous media to improve dispersibility in aromatic solvents and give thermo-responsive and ultraviolet protection properties. *RSC Adv*. 4, 19246-19250 (**2014**).

(97) X. Ren, H. B. Kocer, L. Kou, S. D. Worley, R. M. Broughton, T. Tzou, and T. S. Huang, Antimicrobial polyester. *J. Appl. Polym. Sci.* 109, 2756-2761 (**2008**).

(98) F. W. Czech, R. J. Fuchs, and H. F. Antczak, Determination of mono-, di-, and trichloramine by ultraviolet absorption spectrophotmetry. *Anal. Chem.* 33, 705-707 (**1961**).

(99) J. T. M. Kleinberg, and L. F. Audrieth, Absorption spectrum of aqueous monochloramine solutions. *Anal. Chem*. 26, 1388-1389 (**1954**).

(100) Y. Sun, and G. Sun, Sunflower stalks as adsorbents for color removal from textile wastewater. *Ind. Eng. Chem. Res*. 43, 5015-5020 (**2004**).

(101) Y. Sun, and G. Sun, G. Novel regenerable *N*-Halamine polymeric biocides. I. synthesis, characterization, and antibacterial activity of hydantoin-containing polymers. *J. Appl. Polym. Sci*. 80, 2460-2467 (**2001**).

# List of Publications

1. **A. K. Dutta,** K. Yamada, H. Izawa, M. Morimoto, H. Saimoto, and S. Ifuku, Preparation of chitin nanofibers from dry chitin powder by Star Burst system: Dependence on number of passes. *J. Chitin Chitosan Sci.* 1, 59-64 (**2013**). **[**Chapter 1**]**
2. **A. K. Dutta,** H. Izawa, M. Morimoto, H. Saimoto, and S. Ifuku, Fibers Width and Molecular Weight Studies of *α*-Chitin Nanofibers. *J. Chitin Chitosan Sci.* 1, 192-196 (**2013**). **[**Chapter 1**]**
3. **A. K. Dutta,** H. Izawa, M. Morimoto, H. Saimoto, and S. Ifuku, Simple Preparation of Chitin Nanofibers from Dry Squid pen *β*-chitin Powder by Star Burst System. *J. Chitin Chitosan Sci.*1, 186-191(**2013**). **[**Chapter 2**]**
4. **A. K. Dutta,** H. Izawa, M. Morimoto, H. Saimoto, and S. Ifuku, Novel Preparation of Chitin Nanocrystals by $H_2SO_4$ and $H_3PO_4$ Hydrolysis followed by High-pressure Water Jet Treatments. *J. Chitin Chitosan Sci.* ( **in Press**). **[**Chapter 3**]**
5. **A. K. Dutta,** N. Kawamoto, G. Sugino, H. Izawa, M. Morimoto, H. Saimoto, and S. Ifuku, Simple preparation of chitosan nanofibers from dry chitosan powder by the Star Burst system. *Carbohydr. Polym.* 97, 363-367 (**2013**). **[**Chapter 4**]**
6. **A. K. Dutta,** Mayumi Egusa, H. Kaminaka, H. Izawa, M. Morimoto, H. Saimoto, and S. Ifuku , Facile Preparation of *N*-halamine Chitin Nanofiber for Endowing Antibacterial and Antifungal Properties. (submitted to *Carbohydrate Polymers*) **[**Chapter 5**]**

# Acknowledgements

I would like to express my deep thank to my honorable supervisor, Prof. Hiroyuki Saimoto, Department of Chemistry and Biotechnology, Graduate School of Engineering, for his invaluable guidance, encouragement, and financial support during entire studies at Tottori University, Japan.

The author would like to show his sincere thanks to Dr. Shinsuke Ifuku, Associate Professor, Department of Chemistry and Biotechnology, Graduate School of Engineering, for his insightful suggestions and incessant motivations, especially during the first year, that greatly aided my early research endeavors.

I would like to thank Dr. Hironori Izawa, Assistant Professor, as well as the members of Saimoto Laboratory, Department of Chemistry and Biotechnology, Graduate School of Engineering, for their continuous assistance during the research.

I would like to thank my wife Nilima Dutta, daughter Ahona Dutta, and son Anindya Dutta without whose love, patience, and great sacrifice this work would not have been completed. My mother and late father were always the part of my inspiration. Also thanks to the rest of the family members and friends.

Last but not least, the author is much indebted to the Government of the People's Republic of Bangladesh for giving the opportunity of achieving higher education.